

**Growth and Characterization of Tellurium Single Crystals  
for Applications in Imaging AOTFs**

Final Technical Report

by

**Vitaly B.Voloshinov**

(November 15, 2004)

United States Army

EUROPEAN RESEARCH OFFICE OF THE U.S. ARMY

London, England

Contract number **N 62558-03-M0808** of September 16, 2003

Contractor: Prof. Vitaly B.Voloshinov

Approved for Public Release; Distribution Unlimited

REPORT DOCUMENTATION PAGE			Form Approved OMB No. 0704-0188		
<p>The public reporting burden for this collection of information is estimated to average 1 hour per response, including the time for reviewing instructions, searching existing data sources, gathering and maintaining the data needed, and completing and reviewing the collection of information. Send comments regarding this burden estimate or any other aspect of this collection of information, including suggestions for reducing the burden, to Department of Defense, Washington Headquarters Services, Directorate for Information Operations and Reports (0704-0188), 1215 Jefferson Davis Highway, Suite 1204, Arlington, VA 22202-4302. Respondents should be aware that notwithstanding any other provision of law, no person shall be subject to any penalty for failing to comply with a collection of information if it does not display a currently valid OMB control number.</p> <p><b>PLEASE DO NOT RETURN YOUR FORM TO THE ABOVE ADDRESS.</b></p>					
1. REPORT DATE (DD-MM-YYYY) 16-11-04		2. REPORT TYPE Final Report		3. DATES COVERED (From - To) Sept. 2003 - Sept. 2004; Nov. 15, 2004	
4. TITLE AND SUBTITLE Growth and Characterization of Tellurium Single Crystals for Applications in Imaging AOTFs			5a. CONTRACT NUMBER N 62558-03-M-0808		
			5b. GRANT NUMBER		
			5c. PROGRAM ELEMENT NUMBER		
6. AUTHOR(S) Vitaly B. Voloshinov Professor			5d. PROJECT NUMBER		
			5e. TASK NUMBER		
			5f. WORK UNIT NUMBER		
7. PERFORMING ORGANIZATION NAME(S) AND ADDRESS(ES) Department of Physics, M.V.Lomonosov Moscow State University, 119992 Moscow, Russia (volosh@phys.msu.ru)			8. PERFORMING ORGANIZATION REPORT NUMBER # 4 (Final Report)		
9. SPONSORING/MONITORING AGENCY NAME(S) AND ADDRESS(ES) US Naval Regional Contracting Center, DET London Government Buildings, Block 2, Wing 12, Lime Grove, Ruislip, Middlesex HA4 8BX United Kingdom; (jharvey@usardsguk.army.mil)			10. SPONSOR/MONITOR'S ACRONYM(S)		
			11. SPONSOR/MONITOR'S REPORT NUMBER(S)		
12. DISTRIBUTION/AVAILABILITY STATEMENT Distribution unlimited					
13. SUPPLEMENTARY NOTES					
14. ABSTRACT The Final Report summarizes results of the research carried out in Russia, in M.V.Lomonosov Moscow State University and in A.F.Ioffe Physical-Technical Institute, St. Petersburg, during the period September 16, 2003 – September 15, 2004. The activities were concentrated on fabrication and characterization of physical properties of tellurium specimen grown in the Ioffe Institute under the conditions of the Contract. The theoretical investigation carried out in Moscow University according to the Contract resulted in detailed information about acoustic wave propagation in the crystal. The investigation was also concentrated on study of photoelastic and acousto-optic properties of the material. Selection of geometry of light and sound interaction optimal for the application in the imaging filter was performed in the University. On base of the theoretical analysis, a prototype of acousto-optic cell was fabricated in the Ioffe Institute. Anisotropic diffraction of infrared optical radiation was registered in the acousto-optic cell.					
15. SUBJECT TERMS Acousto-optics, tellurium, tunable acousto-optic filter, anisotropic diffraction, phase velocity of ultrasound, group velocity of ultrasound, wide-angle interaction geometry, acousto-optic figure of merit					
16. SECURITY CLASSIFICATION OF:			17. LIMITATION OF ABSTRACT  UU	18. NUMBER OF PAGES  40	19a. NAME OF RESPONSIBLE PERSON V.B.Voloshinov
a. REPORT U	b. ABSTRACT U	c. THIS PAGE U			19b. TELEPHONE NUMBER (Include area code) 7-095-939-4404

## Abstract

The Final Report summarizes results of the research carried out in Russia, in M.V.Lomonosov Moscow State University and in A.F.Ioffe Physical-Technical Institute, St. Petersburg, during the period September 16, 2003 – September 15, 2004. The activities were concentrated on fabrication and characterization of physical properties of tellurium specimen grown in the A.F.Ioffe Institute under the conditions of the Contract. The theoretical investigation carried out in Moscow University according to the Contract resulted in detailed information about acoustic wave propagation in the crystal. The investigation was also devoted to study of photoelastic and acousto-optic properties of the material. Geometry of light and sound interaction optimal for the application in the imaging filter was found. On base of the grown crystal and the performed theoretical analysis, acousto-optic cell was fabricated in the A.F.Ioffe Institute. Anisotropic diffraction of infrared optical radiation was observed in the acousto-optic cell. Registered characteristics of the interaction in the crystal were in agreement with the predictions of the theory.

**Key words:** acousto-optics, tellurium, tunable acousto-optic filter, anisotropic diffraction, phase velocity of ultrasound, group velocity of ultrasound, wide-angle interaction geometry, acousto-optic figure of merit

## TABLE OF CONTENTS

1.	Introduction .....	5
2.	Physical properties of tellurium .....	6
3.	Acoustic wave propagation in tellurium single crystal . . . . .	10
4.	Photoelastic effect in the material. . . . .	15
5.	Acousto-optic figure of merit in tellurium .....	18
6.	Results of calculation of acousto-optic effect in tellurium .....	19
	a) Interaction in the plane $YZ$ .....	19
	b) Interaction in the plane $X+30^0$ .....	24
7.	Trade-off between figure of merit and optical propagation direction .....	29
8.	Summary of results of calculation .....	39
9.	Growth and characterization of tellurium specimens. . . . .	40
10.	Conclusions .....	43
	Literature cited .....	44

## 1. Introduction

Light diffraction by acoustic waves in crystals is the fundamental effect that is widely used for control of optical radiation [1-4]. As known, the acousto-optic (AO) effect finds many applications in Physics, in Optical Engineering and Information Processing, as well as in Laser Technology, in Ecology, Medicine, Military Sciences, etc. Acousto-optic instruments (light modulators, deflectors and filters) are characterized by high quick-action, reliability, electronic control, low driving power and relatively simple design.

The commercially available acousto-optic instruments are capable of operation in visible and near IR ranges of spectrum [1-4]. The majority of these instruments utilize the single crystal of paratellurite ( $\text{TeO}_2$ ). This crystal is known for the extraordinary high value of AO figure of merit  $M_2 = 1200 \cdot 10^{-18} \text{ s}^3/\text{g}$  [1-5] that results in low RF driving power levels, e.g. of the order of  $P = 0.1$  Watt in the visible light. Unfortunately, this crystal is transparent in the infrared only at the wavelengths  $\lambda$  shorter than 4.5  $\mu\text{m}$ . Thus, the material is not suitable for control of optical radiation in the middle and far infrared range of spectrum at the wavelengths  $\lambda = 8 - 12 \mu\text{m}$  [6-30].

Development of a tunable imaging filter operating in the middle and long infrared region of spectrum appeared to be a very complicated problem. The main reason for the difficulty is that the diffraction efficiency in an acousto-optic instrument is proportional to  $\lambda^{-2}$  [1-4]. Due to this characteristic feature, requirements on the RF driving power increase as  $\lambda^2$ . Therefore, an AO material, which is as effective in the infrared as  $\text{TeO}_2$  in the visible light, should possess the AO figure of merit about  $M_2 = 200\,000 \cdot 10^{-18} \text{ s}^3/\text{g}$ . At present, there are no such materials in Acousto-Optics [1-4].

List of the acousto-optic materials suitable for the application in the infrared region is limited to a few crystals: TAS ( $\text{Ti}_3\text{AsSe}_3$ ) [7], calomel ( $\text{Hg}_2\text{Cl}_2$ ), mercury bromide ( $\text{Hg}_2\text{Br}_2$ ) [10-15] and tellurium (Te) [6, 15-22]. The single crystal of germanium may not be applied in the imaging filters because of absence of birefringence. Moreover, only TAS and calomel crystals have been used to demonstrate the possibility to process images in the long infrared region of spectrum [11,12]. Calomel seems to be slightly superior to TAS due to the larger birefringence of the material. However, both materials are characterized in the infrared by relatively poor acousto-optic efficiency because their figure of merit is limited to  $M_2 = 4500 \cdot 10^{-18} \text{ s}^3/\text{g}$  [7,10-

12], i.e. 50-100 times less than required.

In this respect, tellurium attracts particular attention of designers because of its extremely high figure of merit. According to conclusions of the references [20-22], the figure of merit in tellurium may exceed the magnitude  $M_2 = 500\,000 \cdot 10^{-18} \text{ s}^3/\text{g}$  that is up to 100 times better than in TAS and calomel. However, although tellurium has been known for decades, the material has not been investigated in details, especially if the imaging acousto-optic applications are taken into the consideration. For example, the extraordinary high acousto-optic figure of merit of the material seems rather doubtful [29-31] because only once experiments with the crystal confirmed that the figure of merit of the crystal was really high [30]. However, the high value was observed not in a filter but deflector configuration of the crystal. That is why, a detailed study of tellurium single crystals and analysis of the possibility to apply the material for optical radiation control in the infrared has been one of the goals of the research program carried out according to the Grants of the Technical Research Institute, Virginia and the ARL, Maryland [32-34]. The present Final Report summarizes results of the theoretical and experimental investigation of the crystal. The research was carried out in M.V.Lomonosov Moscow State University and in A.F.Ioffe Physical-Technical Institute in St. Petersburg during the recent year. Preliminary results of the investigation have been presented in June 2004 at the Joint US-Russian Partnership Workshop CELO-2004 "Communication, Electronics, Lasers and Optics" in St. Petersburg, Russia [35].

## 2. Physical properties of tellurium

Single crystal of tellurium is an element of the 6-th group in the periodic Mendeleev Table of chemical elements [3,4,8,9,24,25]. Tellurium possesses the order number of 52. The crystal belongs to the class of crystalline materials  $D_3$  of the trigonal system. A helical "screw" axis of the third order is the basic element of symmetry of the material. This axis is usually defined as the  $C$ -axis or  $Z$ -axis, which is exactly the optical axis of the crystal. The material also possesses 3 equivalent crystalline axes  $X_1$ ,  $X_2$  and  $X_3$  of the second order. These three axes are situated in the basic plane at the angles  $120^\circ$  with respect to each other. There exist two twin modifications of the crystal. According to the definitions of Schonflies, these modifications are the **right** (clockwise) screw modification  $D_3^4$  and the **left**, i.e. the counter-clockwise screw modification  $D_3^6$  of the material [17-22].

Atoms of tellurium form, with respect to the helical axis  $Z$ , some kind of spiral chains. A spatial period of each of the chains is equal to 3 atoms so that the forth atom is situated above the first one. This peculiarity of the lattice composition is illustrated in Fig. 1. The chains are packed in a hexagonal prism. As found, the crystalline lattice does not possess a center of symmetry. The two modifications of tellurium differ by directions of the screw orientation of the spirals. These modifications also differ by optical activity and by shape of a line of a nuclear magnetic resonance. It should be noted that the specimens of tellurium grown in accordance with the requirements of the present Contract, belong to the **left**, i.e. to the **counter-clockwise** screw system.

Elementary cell of the crystal consists of 3 atoms. It was found that a covalent type of atomic bond is typical of the chains while the Van der Waals and, in part, the covalent bond is typical of the chains. That is why, the crystals of tellurium may be are easily cut along the planes (1010) that are parallel to the axis  $Z$ .

Melting temperature of tellurium is equal to  $t = 452^0$  C. Density of the material at the temperature  $t = 20^0$  C and the hardness, according to Mohs, are correspondingly equal to  $\rho = 6.25$  g/cm<sup>3</sup> and 2.0-2.5. Finally, the requirements of the crystalline symmetry indicate that only 6 independent elastic coefficients  $c_{ij}$  exist in the material. Two sets of the elastic coefficients were considered during the Research Program. The reference [25] proposes the following values of the coefficients

$$\begin{aligned} c_{11} &= (3.76 - 1.65 \cdot 10^{-3} \cdot T) \cdot 10^{11} \text{ dyn/cm}^2; & c_{12} &= (0.94 - 0.23 \cdot 10^{-3} \cdot T) \cdot 10^{11} \text{ dyn/cm}^2; \\ c_{13} &= (2.88 - 1.29 \cdot 10^{-3} \cdot T) \cdot 10^{11} \text{ dyn/cm}^2; & c_{14} &= +(1.43 - 0.645 \cdot 10^{-3} \cdot T) \cdot 10^{11} \text{ dyn/cm}^2; \\ c_{33} &= (7.85 - 2.10 \cdot 10^{-3} \cdot T) \cdot 10^{11} \text{ dyn/cm}^2; & c_{44} &= (3.55 - 1.43 \cdot 10^{-3} \cdot T) \cdot 10^{11} \text{ dyn/cm}^2, \end{aligned}$$

where the temperature of the crystal is included in the limits  $T = 100-300$  K . It should be pointed out that, in this Report, the coefficient  $c_{14}$  is taken positive and it is relatively large. The sign “+” of the coefficient is typical only of the left modifications of the crystal while the large value of the coefficient  $c_{14}$  indicates that the crystal possesses low grade of crystalline symmetry. During the research, another set of elastic constants was also considered [34]. It was obtained by averaging of all data on tellurium available in scientific literature [6, 17-22, 29,30]:

$$\begin{aligned} c_{11} &= 3.42 \cdot 10^{11} \text{ dyn/cm}^2 & (3.5\%); & & c_{12} &= 0.98 \cdot 10^{11} \text{ dyn/cm}^2 & (7.4\%); \\ c_{13} &= 2.32 \cdot 10^{11} \text{ dyn/cm}^2 & (2.6\%); & & c_{14} &= 1.26 \cdot 10^{11} \text{ dyn/cm}^2 & (8.4\%); \end{aligned}$$

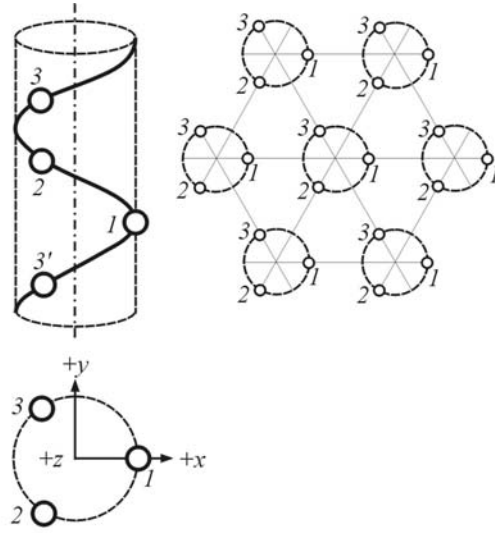


Figure 1. Spatial structure of tellurium single crystal

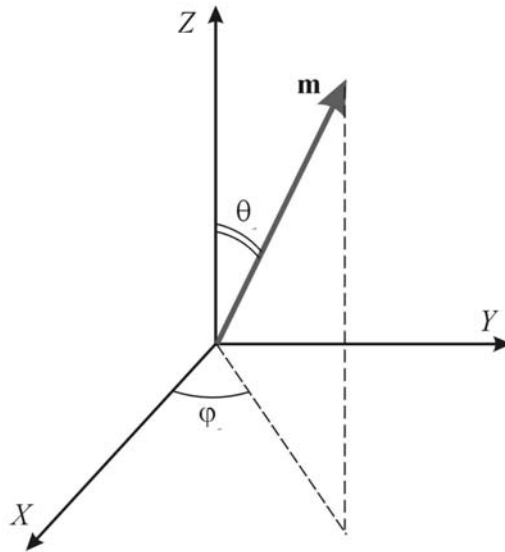


Figure 2. Direction of acoustic wave normal

$$c_{33} = 7.06 \cdot 10^{11} \text{ dyn/cm}^2 \quad (1.8\%); \quad c_{44} = 2.85 \cdot 10^{11} \text{ dyn/cm}^2 \quad (4.4\%).$$

In the parentheses, a mean-square discrepancy value is included. This discrepancy determined the precision of the calculations presented in the reference [34]. As seen, the difference between the two sets of values is not so noticeable. In this Report, the first set of the coefficients was used, while the previous analysis [32-34] had been based on the second set of the coefficients.

The strong anisotropy of the crystal causes the unusual physical feature of the material that the elastic limit depends on direction of application of strain. A plastic deformation that exists even at the temperatures up to  $T = 77$  K is accompanied by appearance of various types of dislocations. It was found that best specimen of tellurium possessed density of the dislocations of the order  $10^3 \text{ cm}^{-2}$ . However, small strain applied to the crystal may increase the density of the dislocations up to  $10^6 \text{ cm}^{-2}$ . Finally, the deformations about  $3 \cdot 10^{-5}$  resulted in the density of the dislocations as large as  $10^7 - 10^8 \text{ cm}^{-2}$ . It should be stated that the structural disorders in tellurium strongly influence on practically all physical properties of the material.

At the temperature  $T = 300$  K, tellurium has a concentration of the holes about  $p = 10^{16} \text{ cm}^{-3}$ . The crystal may be defined as an intrinsic semiconductor. A decrease of temperature of a specimen is accompanied by a transfer to the region of impurity conduction while usually the material is a p-type hole semiconductor. The transfer temperature  $T_i$  belongs to the range of temperatures  $T_i = 190-210$  K if the concentration of holes is limited to  $p = 10^{14} - 10^{15} \text{ cm}^{-3}$ . Minimum of the conduction is observed at the transfer temperature  $T_i$ . At lower temperatures, the concentration of holes is not changed, however, it begins to grow due to mobility of the carriers, i.e. the electrons. It was found that the mobility of the minority carriers in tellurium is about 2 times higher than the mobility of holes. This ratio is practically not varied with the temperature. It is evident that presence of the defects most strongly influences on the electrical properties of the most pure specimen of tellurium. The defects in the crystal decrease the mobility of the carriers and increase their concentration.

Absence of a center of inversion in the crystalline lattice of tellurium provides existence of a piezoelectric effect. Analysis demonstrates that the single crystal of tellurium is a stronger piezoelectric material than the crystals of CdS, n-InSb and many other materials. Tensor of the piezoelectric constants possesses only 2 independent coefficients  $d_{11}$  and  $d_{14}$ . An electromechanical coupling constant of the crystal is equal to 0.12 if a longitudinal wave is

propagating along the  $X$  axis of the crystal. A shear wave along the axis  $Y$  with a polarization along the axis  $X$  possesses the electromechanical coupling coefficient about 2 times higher 0.27.

Optical properties of the crystal are rather unusual. The crystal is positive, consequently the index of refraction for the ordinary polarized wave  $n_o$  is lower than the index for the extraordinary polarized light  $n_e$ . The material is optically transparent in the range of wavelengths  $\lambda = 5.0 - 20.0$  mkm. Tellurium is also known as one of the materials with the extremely strong optical anisotropy [6,16-22]. The birefringence of tellurium  $\Delta n = n_e - n_o$  at the wavelength of light  $\lambda = 10.6$  mkm is equal to 1.4 because the indexes of refraction are as follows:  $n_e = 6.2$  and  $n_o = 4.8$ . The high values of the refractive indexes indicate that the Fresnel reflection coefficient of the crystal is close to  $R = 50\%$  causing poor crystal transparency. For example, a specimen with the thickness 0.22 cm and the concentration of holes  $p = 10^{14} \text{ cm}^{-3}$  at  $T = 300$  K (in the impurity region) possesses the transparency coefficient that does not exceed  $T = 30\%$  for the ordinary polarized light and 15% for the extraordinary polarized radiation. It means that fabrication of a cell on base of tellurium requires application of antireflection coatings.

If optical absorption is considered, it may be stated that the absorption depends on the temperature in a rather peculiar manner. In the range of optical wavelengths  $\lambda = 5 - 10$  mkm, the absorption of the extraordinary polarized radiation increases with temperature while the absorption of the extraordinary polarized beam vanishes. However, it was noticed that, in general, a structural quality of a sample influences the optical transparency of the material. As found, dislocations and defects in the crystal determine such basic parameter of the crystal as the concentration of the carriers.

### 3. Acoustic wave propagation in tellurium single crystal

Acoustic properties of a crystal may be completely described by the coefficients of the elastic tensor  $c_{ijkl}$ . The wave equation of elasto-dynamics leads to the so-called Christoffel equation [8,9]

$$\rho V^2 u_i = \Gamma_{il} u_l, \quad (1)$$

where  $u_l$  ( $l = 1, 2, 3$ ) are the components of the displacement vector  $\mathbf{u}$ . The equation (1) enables to calculate the velocities  $V$  being the “eigen values” of the Christoffel tensor

$$\Gamma_{il} = c_{ijkl} m_j m_k \quad (i, j, k, l = 1, 2, 3). \quad (2)$$

Here  $m_j$  are the components of the unit vector of the acoustic wave normal  $\mathbf{m}$ . It is convenient to determine direction of the acoustic wave normal  $\mathbf{m}$  in the system of the crystalline axes  $X$ ,  $Y$  and  $Z$  by the azimuth angle  $\varphi_a$  measured in the  $XY$  plane from the  $X$  axis and by the polar angle  $\theta_a$  measured with respect to the  $Z$  axis. The direction of the wave normal and the Cartesian axes are shown in Fig. 2. In this case, the components of the unit vector  $\mathbf{m}$  may be written as

$$m_1 = \cos(\varphi_a) \sin(\theta_a); \quad m_2 = \sin(\varphi_a) \sin(\theta_a); \quad m_3 = \cos(\theta_a). \quad (3)$$

Thus, specifying an arbitrary direction of the vector  $\mathbf{m}$ , one can find the magnitudes of the three phase acoustic velocities  $V_1$ ,  $V_2$  and  $V_3$ . The velocity values are found as roots of the secular equation

$$|\Gamma_{il} - \rho V^2 \delta_{il}| = 0, \quad (4)$$

where  $\delta_{il}$  is the Kronecker symbol. Each velocity  $V$  corresponds to an eigenvector  $\mathbf{u} = u\mathbf{r}$  determining a displacement in the acoustic wave while  $\mathbf{r}$  is a unit vector of polarization of the acoustic wave polarization. It is known that the three vectors  $\mathbf{r}$  are mutually orthogonal.

Calculation of the acoustic velocities  $V$  and the polarization vectors  $\mathbf{r}$  is not the only problem that is of importance during the analysis of the acousto-optic interaction. It is also necessary to know the group velocities  $V^e$  and the walk-off angles  $\alpha$ , i.e. the angle between phase and the group velocities of ultrasound. For each phase velocity value  $V$ , the group velocity components  $V_i^e$  may be found from the equation [8,9]

$$V_i^e = \frac{1}{\rho V} c_{ijkl} r_j r_l m_k. \quad (6)$$

Writing down the group velocity vector as  $\mathbf{V}^e = V^e \mathbf{s}$ , where  $\mathbf{s}$  is the ray vector of the acoustic wave, one can determine the walk-off angle

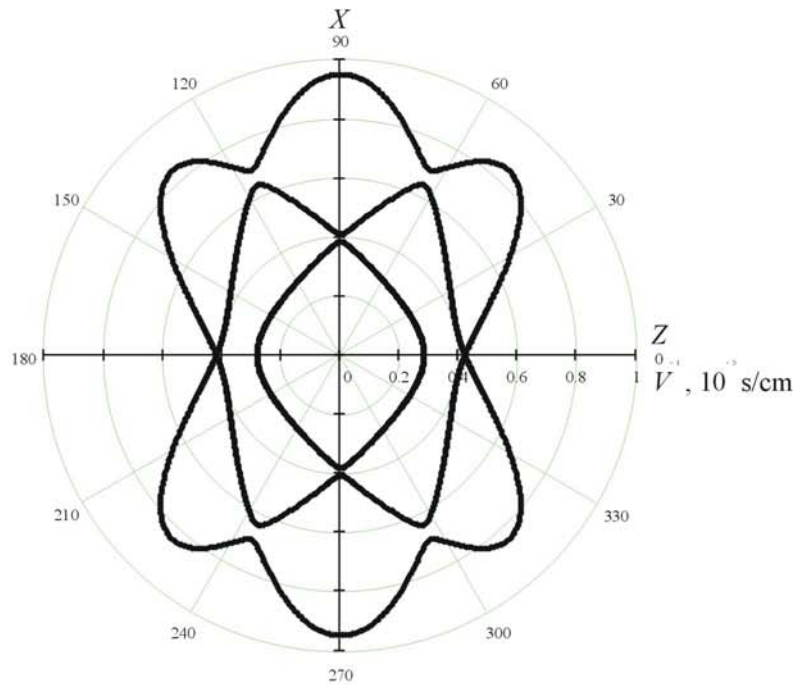


Figure 3. Acoustic slowness polar diagram for the plane  $XZ$  as well as for the planes  $XZ+60^\circ$ ,  $XZ+120^\circ$ ,...

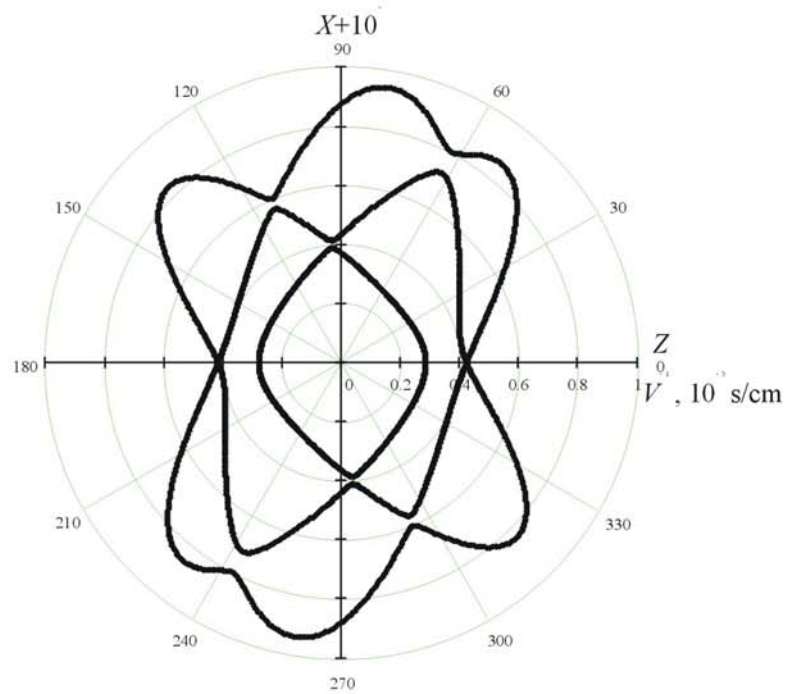


Figure 4. Acoustic slowness polar diagram for the plane  $XZ+10^\circ$  as well as for the planes  $XZ+50^\circ$ ,  $XZ+130^\circ$ ,...

$$\cos \alpha = \mathbf{s} \cdot \mathbf{m} = s_i m_i. \quad (7)$$

In this report, the acoustic parameters of the waves were calculated by means of a specially developed computer software. The computer program made it possible to find the phase and the group velocities of all the three acoustic waves, the walk-off angles of these modes, orientation of the polarization vector  $\mathbf{r}$  and directions of the ray vector  $\mathbf{s}$  in the crystal. Basic results of the calculation will be presented and discussed below.

Figure 3 shows cross section of the slowness surface in tellurium by the crystallographic plane  $XZ$ . In the figure, the polar angle  $\theta_a$  is evaluated relatively to the  $Z$  axis in the counter-clockwise direction while the slowness  $1/V$  is evaluated along a radius. The external curve in Fig. 3 corresponds to the slowest acoustic mode. This mode is of a particular interest because the AO figure of merit of the crystal is proportional to  $V^{-3}$  [1-4].

As follows from the figure, the minimum value of the acoustic velocity is observed if the acoustic wave propagates along the  $X$  axis. The phase velocity value is equal in this case to  $V = 1.05 \cdot 10^5$  cm/s. This mode is a pure shear wave because the acoustic polarization vector is directed at the angle  $61^\circ$  to the  $Z$  axis in the  $YZ$  plane. As for the  $Z$  axis itself, it is not interesting for the acousto-optic applications because of the relatively high values of the acoustic velocities.

As for data in Fig. 4 - Fig. 6, they demonstrate the cross-section of the slowness surface by the planes rotated round the  $Z$  axis at the angles  $10^\circ$ ,  $20^\circ$  and  $30^\circ$  accordingly. The regular trend of the waves propagation is quite clear. The minimum value of the phase velocity  $V = 1.05 \cdot 10^5$  cm/s is obtained in the plane  $X + 30^\circ$  at the angle  $\theta_a = 61.5^\circ$ . The magnitudes of the velocity and the direction of polarization are similar to the case of the slow acoustic mode along the  $X$  axis in Fig. 3. A further growth of the azimuth angle  $\varphi_a$  results in the polar diagrams identical to that shown in Fig. 4 and Fig. 5. For example, the diagram for the angle  $\varphi_a = 40^\circ$  coincides with the diagram for the case  $\varphi_a = 20^\circ$ , the diagram for  $\varphi_a = 50^\circ$  is identical to the diagram typical of the angle  $\varphi_a = 10^\circ$ . As for the angle  $\varphi_a = 60^\circ$ , one obtains the diagram presented in Fig. 7. Moreover, in the range of the angles  $60^\circ < \varphi_a < 120^\circ$ , the diagrams are similar but mirror reflected about the vertical axis  $Z$ . Thus, the acoustic slowness diagrams show a recurrence with respect to the angle  $\varphi$  with the period of  $120^\circ$ . This is quite natural since the axis  $Z$  of tellurium is the three-fold axis of the crystalline symmetry.

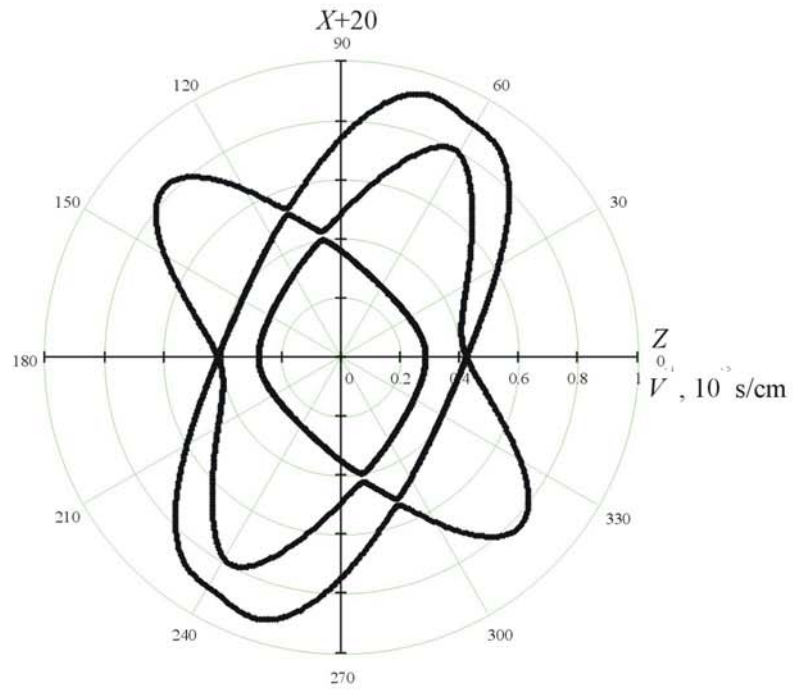


Figure 5. Acoustic slowness polar diagram for the plane  $XZ+20^\circ$  as well as for the planes  $XZ+40^\circ$ ,  $XZ+140^\circ$ , ...

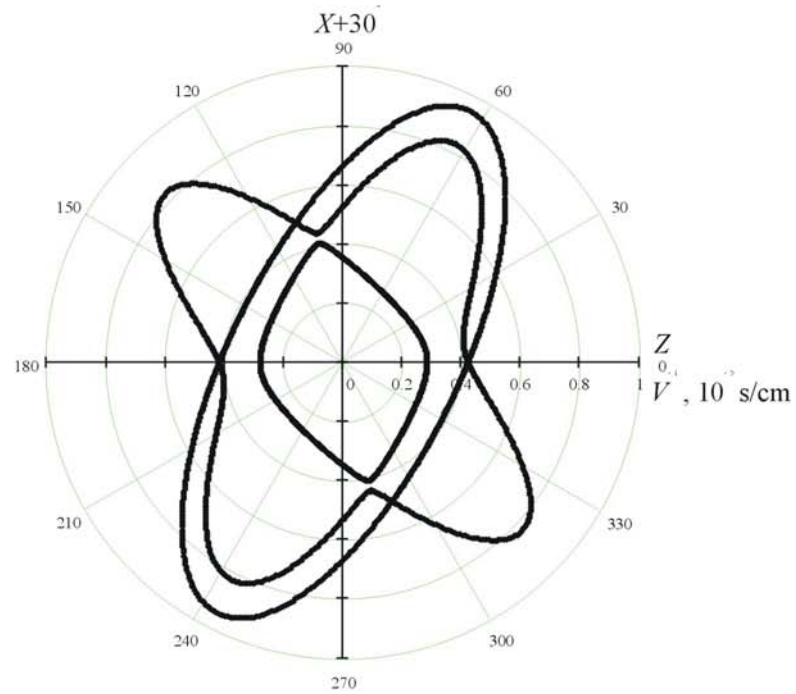


Figure 6. Acoustic slowness polar diagram for the plane  $XZ+30^\circ$  as well as for the planes  $XZ+150^\circ$  and  $XZ+270^\circ$

In order to fulfill the analysis, in Fig. 8, the polar diagram for the plane  $XY$  of tellurium is shown. This diagram possesses the symmetry of the sixth order because the magnitudes of the acoustic phase velocities are repeated in the direction of the angle  $\varphi$  with the period of  $60^\circ$ . As found, the axis  $Y$  is the most non-symmetrical crystallographic axis in the material. Only one acoustic mode is totally pure in this plane. It is the slow shear mode with the velocity  $V = 1.4 \cdot 10^5$  cm/s polarized along the axis  $X$ . The two other acoustic waves are the quasi-shear mode with the velocity  $V = 1.72 \cdot 10^5$  cm/s and the quasi-longitudinal mode with the velocity  $V = 2.66 \cdot 10^5$  cm/s. These modes are polarized in the  $YZ$  plane of the crystal. These waves are characterized by a considerable walk-off angle equal to  $46^\circ$ ,  $48^\circ$  and  $37^\circ$  respectively.

Since the walk-off angles  $\alpha$  dramatically influence on characteristics of the AO devices, the walkoff angle has been calculated for the examined directions of acoustic propagation in the crystal [21, 33,34]. It was shown, as a result of the analysis, that the single crystal of tellurium is an extremely anisotropic elastic medium because the walkoff angles in the  $YZ$  plane may be as large as  $48^\circ$ . In general, the walkoff angles in tellurium may be large. They are limited by the magnitude  $57^\circ$  [21,34,35].

#### 4. Photoelastic effect in the material

It is known that the photoelastic effect in a medium is described as a change of refractive indexes induced by elastic strain. If the acoustic eigenvectors  $\mathbf{u}$  are known, one can calculate the components of the elastic deformation tensor or strain tensor  $\widehat{\mathbf{S}}$ :

$$S_{ij} = Ku \frac{r_i m_j + r_j m_i}{2} = \sqrt{\frac{2P_a}{\rho V^3 l b}} \cdot \frac{r_i m_j + r_j m_i}{2}, \quad (8)$$

where  $K = \Omega/V = 2\pi f/V$  is the acoustic propagation constant,  $\Omega$  - is the cycle frequency of sound,  $P_a$  is the acoustic power and  $l \times b$  is the cross-section of the acoustic beam. In the above equation,  $l$  is the acoustic beam width evaluated in the AO interaction plane.

The photoelastic effect is described as variations of the non-permittivity tensor  $\widehat{\mathbf{B}}$  induced by the elastic strain  $\widehat{\mathbf{S}}$  [1,3,4]:

$$\Delta B_{ij} = p_{ijkl} S_{kl}, \quad (i,j,k,l = 1,2,3) \quad (9)$$

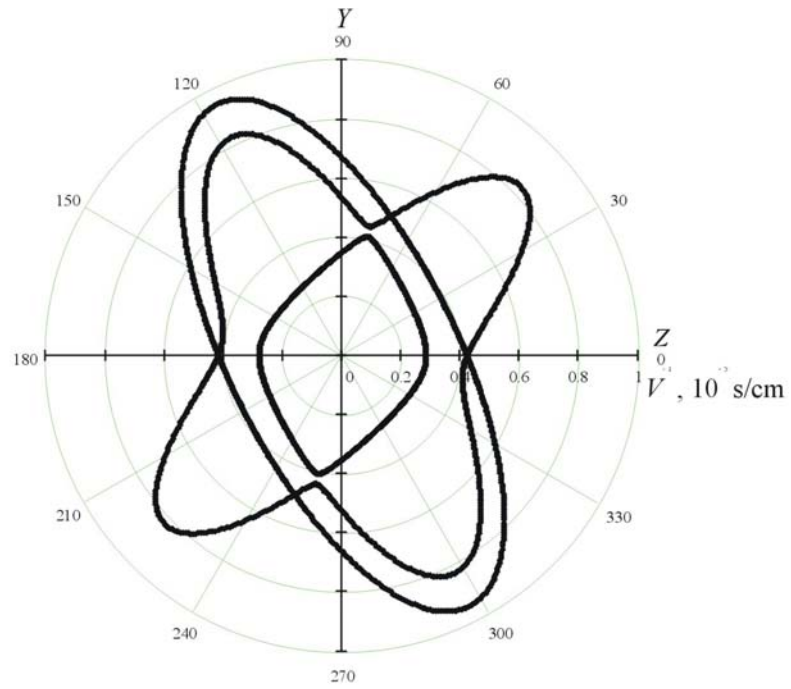


Figure 7. Acoustic slowness polar diagram for the plane  $YZ$

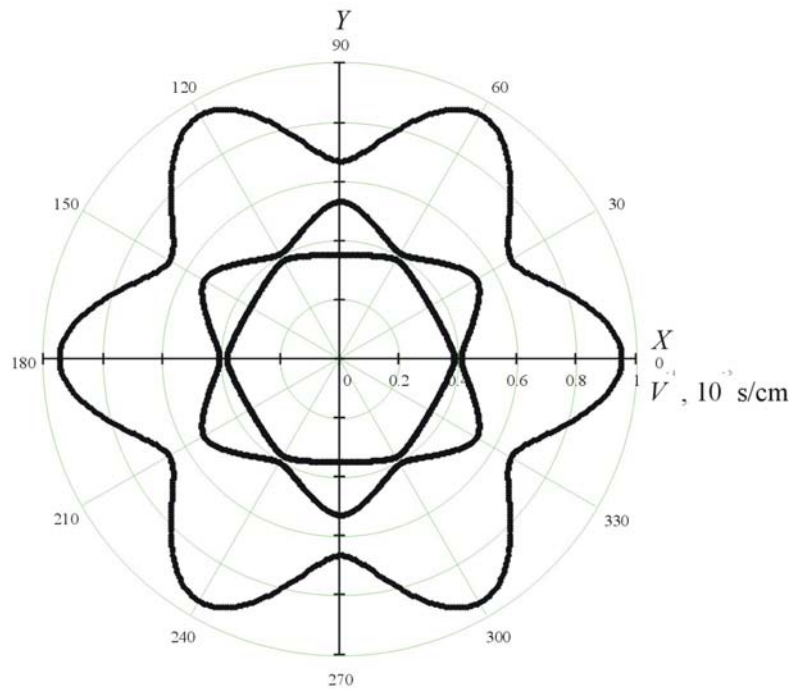


Figure 8. Acoustic slowness polar diagram for the plane  $XY$

where  $p_{ijkl}$  are the components of the photoelastic tensor  $\hat{\mathbf{p}}$ . The matrix of the photoelastic coefficients  $p_{\alpha\beta}$  ( $\alpha, \beta = 1, \dots, 6$ ) of the single crystal of tellurium may be found in literature [22]. In the calculations presented below, the following values of the coefficients have been used [22]:

$$\begin{aligned} p_{11} &= 0.164; & p_{12} &= 0.138; & p_{13} &= 0.146; & p_{14} &= -0.04; & p_{21} &= 0.138; \\ p_{31} &= -0.086; & p_{33} &= 0.038; & p_{41} &= 0.28; & p_{44} &= 0.14; & p_{66} &= 0.013. \end{aligned}$$

Application of the known components of the strain (8) and of the photoelastic coefficients resulted in the expressions (9) for calculation of variations of the permittivity matrix. It yields the formula for the acousto-optic figure of merit of the crystal

$$M_2^* = \frac{1}{\rho V^3} \frac{\left[ e_i^{(1)} \varepsilon_{ij} \varepsilon_{kl} e_l^{(0)} p_{jkmn} (r_m m_n + r_n m_m) \right]^2}{4n_0 n_1 \cos \vartheta_0 \cos \vartheta_1}, \quad (10)$$

where  $\varepsilon_{ij}$ ,  $\varepsilon_{kl}$  and  $n_0$ ,  $n_1$  are the components of the permittivity matrix and the refractive indexes for the incident and the diffracted beams. The multipliers  $\cos \vartheta_0$  and  $\cos \vartheta_1$  in the formula (10) illustrate the characteristic feature that the incident and the diffracted optical waves pass through the acoustic field obliquely at the angles  $\vartheta_0$  and  $\vartheta_1$ . Therefore, the lengths of the acousto-optic interaction for the incident and the diffracted beams are not equal to each other.

As mentioned, in a real device, the lengths of the interaction are correspondingly equal to  $l/\cos \vartheta_0$  and  $l/\cos \vartheta_1$ . Due to this peculiarity, the figure of merit  $M_2^*$  (10) tends to infinity when the angles of propagation  $\vartheta_0$  and  $\vartheta_1$  approach  $90^\circ$ . Therefore, it is reasonable to introduce, additionally to the coefficient  $M_2^*$ , a "pure" or an "intrinsic" AO figure of merit

$$M_2 = \frac{1}{4n_0 n_1 \rho V^3} \left[ e_i^{(1)} \varepsilon_{ij} \varepsilon_{kl} e_l^{(0)} p_{jkmn} (r_m m_n + r_n m_m) \right]^2 \quad (11)$$

that totally characterizes efficiency of the acousto-optic interaction independently of the interaction length. It is just this value that has been calculated in the present research.

## 5. Acousto-optic figure of merit in tellurium

In the majority of publications devoted to analysis of the acousto-optic effect in crystals, the investigation was limited to the case of the orthogonal acousto-optic interaction when the angles  $\vartheta_0$  and  $\vartheta_1$  were close to zero. In general, this approximation is valid in such devices as modulators, deflectors and spectrum analyzers based on the orthogonal or the quasi-orthogonal geometry of the diffraction [1-4]. On the contrary, the acousto-optic filters may utilize the interaction geometry characterized by the propagation angles  $\vartheta_0$  and  $\vartheta_1$  as large as dozens of degrees and in some cases even up to  $90^\circ$  [26-28]. Therefore, a more detailed analysis of the acousto-optic diffraction becomes necessary in the case of the trigonal material.

There is one more aspect that should be taken into the consideration during the analysis. It was found that the angles  $\vartheta_0$  and  $\vartheta_1$  may not be specified independently of each other because they are coupled by the condition of phase matching [1-4]. In other words, once a value of the incidence angle  $\vartheta_0$  is chosen, a value of the acoustic frequency  $f$  should be found. It is clear that this frequency value satisfies the condition of Bragg matching. On base of the coupled magnitudes of the angle  $\vartheta_0$  and the frequency  $f$ , one can calculate the angle  $\vartheta_1$  corresponding to the diffracted beam.

The computer software specially developed for the analysis of the acousto-optic interaction in the tellurium single crystal included the following subprograms:

- 1) calculation of all characteristics of acoustic waves in tellurium. The calculation provides data on the magnitudes of the acoustic phase and group velocities, the walkoff angle and the direction of acoustic polarization;
- 2) calculation of all characteristics of the optical waves, i.e. the indexes of refraction for the ordinary and extraordinary polarized rays, as well as the polarization vectors;
- 3) calculation of the Bragg angles of light incidence as a function of the acoustic frequency for a chosen direction of light and sound propagation;
- 4) calculation of the AO figure of merit for a chosen crystal cut.

The above described method of analysis required complicated analytical and routine computer calculations. In the Final report, only those results of the calculation will be discussed that are of interest for the particular application in the imaging acousto-optic cell. The calculations were carried out only for the particular regime of the anisotropic diffraction because

only this type of the acousto-optic interaction is applied in the imaging filters. For simplicity, the incident light during the analysis was chosen extraordinary polarized and the optical wavelength of radiation was taken equal to  $\lambda = 10.6 \text{ mkm}$ .

## 6. Results of calculation of acousto-optic effect

On base of the carried out analysis of the acoustic slowness in the single crystal of tellurium, it was reasonable to conclude that the most interesting cases, from the point of view of the application, were related to the slow shear acoustic waves. Moreover, the analysis should be concentrated on the waves propagating in the crystalline planes including, one the one hand, the optical axis  $Z$  and, on the other hand, rotated with respect to the axis  $\mathbf{X}$  at the angles  $\varphi_a = 30^\circ$  (the plane  $X+30^\circ$ ) and  $\varphi_a = 90^\circ$  (the plane  $YZ$ ). Due to the crystalline symmetry, the planes  $\varphi_a = 150^\circ$  (the plane  $X+150^\circ$ ) and other symmetrical in the trigonal crystal planes must also be examined. It is evident that the choice of the slow shear wave makes it reasonable to expect observation of much higher values of the figure of merit values because of the dependence  $M_2 \propto V^{-3}$ . The second reason that makes this slow shear elastic wave very attractive for the application is the unique feature that it is a pure mode. Therefore, there will be no problems of generation of these waves in a crystal because their polarization is always directed orthogonal to the plane of the propagation.

Unfortunately, the strong anisotropy of the material results, for all these waves, in the large values of the walkoff angle approaching the magnitudes up to  $\alpha = 46^\circ$ . In order to decrease the influence of the acoustic anisotropy on operation parameters of the acousto-optic devices, it was necessary to choose, in the design of the instruments, the planes of interaction that included the optical axis  $Z$  of the crystal. Moreover, special attention was devoted to the cases of the acoustic propagation characterized by the absence of the energy walkoff angle at  $\alpha = 0$ .

### a) Interaction in the plane $YZ$

Data on the acoustic slowness presented in Fig. 7 demonstrate that the minimal absolute value of the phase velocity of the waves is obtained at the acoustic propagation angle  $\vartheta_a = 116.5^\circ$ . This minimal velocity value in tellurium occurs equal in to  $V = 1.05 \cdot 10^{-5} \text{ cm/s}$  while the acoustic walkoff

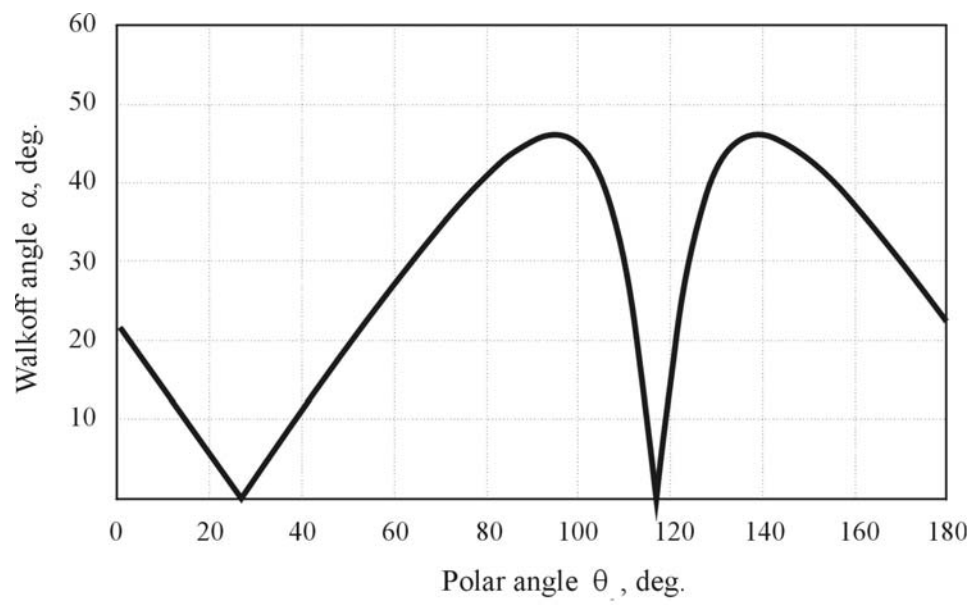


Figure 9. Dependence of acoustic walkoff angle on direction of wave vector in  $YZ$  plane

angle for the chosen elastic mode is approximately limited to zero  $\alpha \approx 0$ . The latter conclusion may be derived from the dependence presented in Fig. 9.

Spatial structure of the acousto-optic effect, i.e. distribution of the figure of merit values over the range of the incidence angles for the slow-shear acoustic mode is presented in Fig. 10. The calculation was performed in the interval of the optic propagation angles varying from  $\varphi_o = 0$  to  $\varphi_o = 90^0$  and from  $\mathcal{G}_o = 0$  to  $\mathcal{G}_o = 180^0$ . The diagrams (a) and (b) in Fig. 10 correspond to the low-frequency and high-frequency branches of the anisotropic diffraction. It follows from the calculations and from the diagrams that the maximum value of the acousto-optic figure of merit equal to  $M_2 = 33\,090 \cdot 10^{-18} \text{ s}^3 / g$  is observed during propagation of the extraordinary polarized optical beam at the angles  $\varphi_o = 90^0$  and  $\mathcal{G}_o = 98^0$  with respect to the crystalline axes  $X$ ,  $Y$  and  $Z$ . In other words, the incident optical beam should be directed in the plane  $YZ$  of tellurium at the angle  $18.5^0$  with respect to the acoustic beam. The particular value of the Bragg angle of incidence  $\mathcal{G}_B = 71.5^0$  corresponds to this geometry of the interaction. The calculations prove that the diffraction angle for the ordinary polarized ray in the examined geometry is equal to  $\mathcal{G}_d = 65.8^0$  while the frequency of ultrasound is limited to  $f = 150.1 \text{ MHz}$ .

The vector diagram corresponding to the optimal interaction geometry is shown in Fig. 11. The diagram is drawn for the case of the extraordinary polarized optical beam. Analysis demonstrates that there exists a region of the optical incidence angles from  $\mathcal{G}_o = 17^0$  to  $\mathcal{G}_o = 62^0$ , in which the Bragg matching condition may not be satisfied and the momentum matching vector diagram may not be drawn. In the limit points of this region, the Bragg angle reaches a minimal or a maximal value. On the contrary, the angle of diffraction at the limit points is equal to zero.

Figure 12 shows the dependence of the Bragg angle on the acoustic frequency. The dependence is valid in the whole range of the acousto-optic interactions taking place in the plane  $YZ$ . The lines (e) correspond to the interaction of the extraordinary polarized wave while the lines (o) describe the ordinary polarized light. The low-frequency fragments of the angular characteristics, i.e. at the acoustic frequencies of most practical interest  $f \leq 400 \text{ MHz}$ , are plotted in Fig. 13 by thin lines. The curves are touching the ordinate axis at the point  $\mathcal{G}_B = -26.5^0$  that corresponds to propagation of light along the optical axis  $Z$ . The extreme

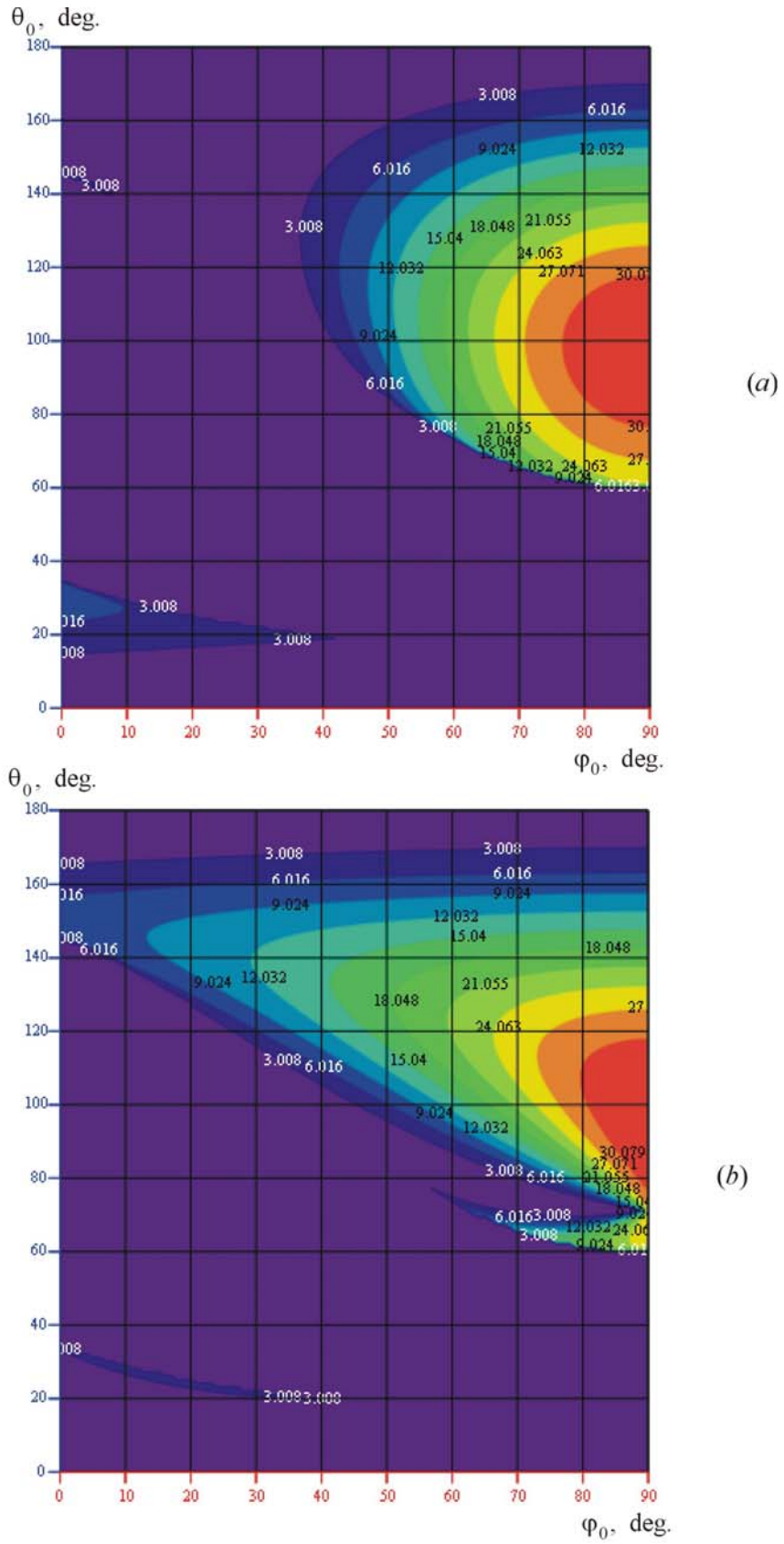


Figure 10. Spatial structure of AO effect in YZ plane ( $\theta = 116.5^\circ$ )

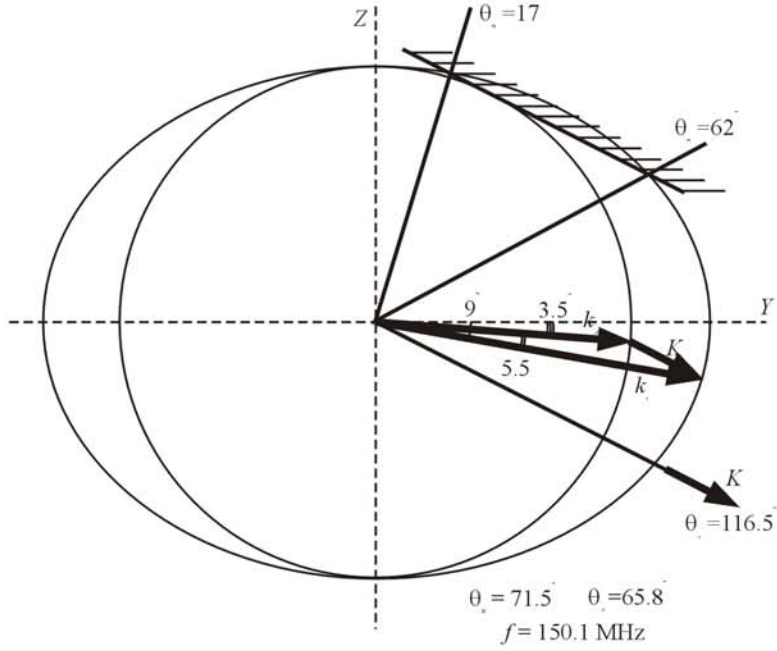


Figure 11. Wave vector diagram for optimal interaction in  $YZ$  plane at  $\theta_z = 116.5$

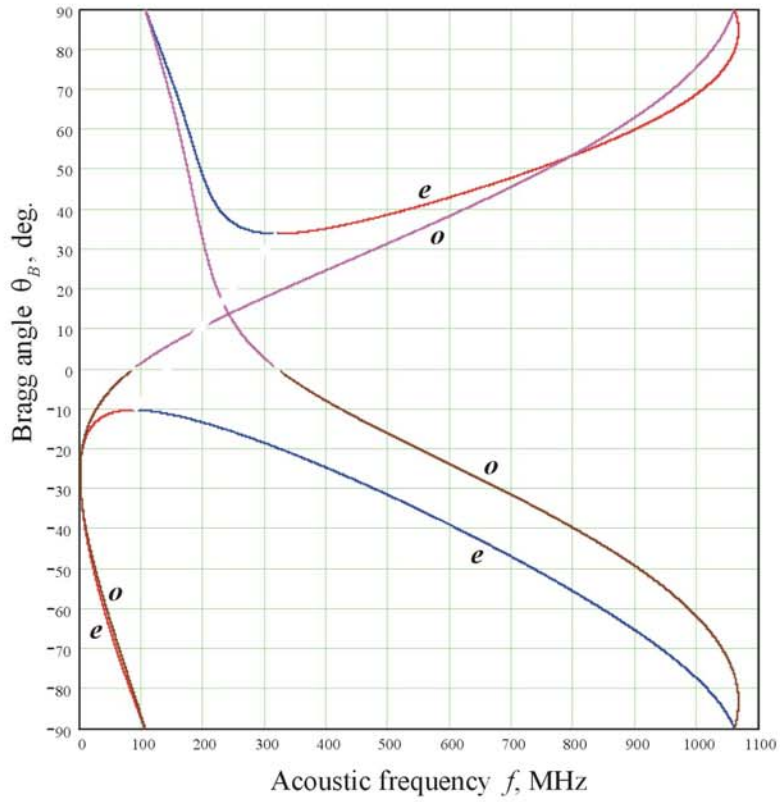


Figure 12. Frequency dependence of Bragg angles in  $YZ$  plane

magnitudes of the Bragg angle for the extraordinary polarized light are observed at the points  $f = 88$  MHz (the maximum value) and  $f = 320$  MHz (the minimum value). It is seen that the diffraction angle at these acoustic frequencies is equal to zero. As found by the calculations, at the frequency of ultrasound  $f = 105$  MHz, the collinear interaction takes place in the crystal because  $\mathcal{G}_B = 90^\circ$ . Analysis demonstrates that an optical beam in the collinear case propagates through the crystal at the angle  $\mathcal{G}_o = 116.5^\circ$  with respect to the optical axis.

The bold red curve in Fig. 13 demonstrates the dependence of the acousto-optic figure of merit  $M_2$  on the acoustic frequency. The bold line possesses as much as two branches, therefore the following definitions were used in the investigation. The blue colour in Fig. 13 marks the lower branch of the diffraction efficiency dependence and the upper branch is marked by the red colour. The corresponding branches of the frequency dependence  $\mathcal{G}_B(f)$  are marked in a similar manner. During the calculation of the figure of merit, both diagrams in Fig. 10 were taken into the account. In order to ensure a proper interpretation of the obtained results, it is necessary to remember that the acousto-optic effect is a reciprocal effect with respect to a direction of light propagation. That is why, the directions described by the Bragg angles  $\mathcal{G}_B = 90^\circ + \psi$  and  $\mathcal{G}_B = -90^\circ + \psi$  result in equal magnitudes of the acousto-optic effect.

It follows from data in Fig. 11 and Fig. 13 that the maximum value of the acousto-optic effect in  $YZ$  plane of tellurium are obtained in the interaction geometry that is close to the collinear diffraction when the Bragg angle is equal to  $\mathcal{G}_B = 71.5^\circ$ . In the pure collinear case, the figure of merit is equal to  $M_2 = 30\,500 \cdot 10^{-18} \text{ s}^3 / g$  that is only about 6% less than the maximum value in the  $YZ$  plane. However, in both cases, the considered interaction geometry is not the wide angle diffraction applied in the imaging filters [1-4]. Consequently, the investigated regime of the anisotropic diffraction may be recommended for application only in filters for processing of collimated optical beams [26-28]. In other words, the acousto-optic interaction in  $YZ$  plane is not good for the imaging purposes.

### **b) Interaction in the plane $X+30^\circ$**

From the point of view of Acoustics, the plane  $X+30^\circ$  possesses only minor differences with respect to the plane  $YZ$  because the acoustic slowness curve in the plane  $X+30^\circ$  is mirror

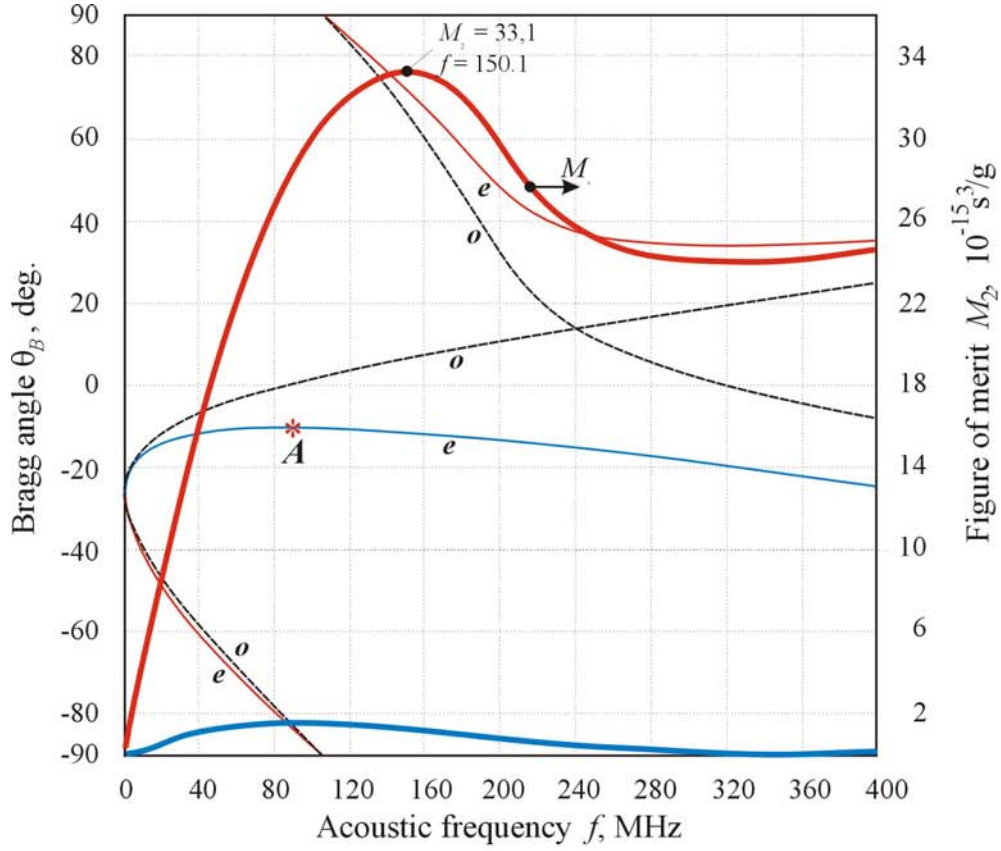


Figure13. Dependence of Bragg angles and figure of merit on acoustic frequency in YZ plane

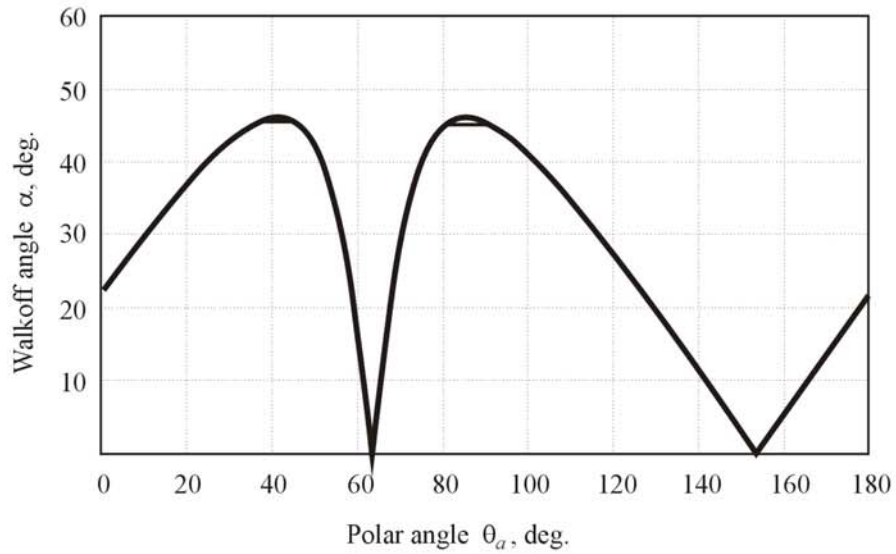


Figure 14. Acoustic walkoff angle in  $X+30^\circ$  plane in tellurium

reflection of the curve in the plane  $YZ$  (Fig. 7). The minimal value of the phase velocity in the plane  $X+30^0$  is also equal to  $V = 1.05 \cdot 10^{-5}$  cm/s, as it takes place in the  $YZ$  plane. However, this minimum velocity value is registered at the acoustic propagation angle  $\vartheta_a = 63.5^0$ . As for the acoustic walkoff angle typical of this elastic mode, it is equal to zero  $\alpha = 0$ , as proved by Fig. 14. All other slow shear acoustic modes in the examined plane are also the pure elastic modes polarized orthogonal to the plane  $X+30^0$ . The maximal value of the walkoff angle  $\alpha = 46^0$  may be obtained at the acoustic propagation  $\vartheta_a = 41^0$  and  $\vartheta_a = 86^0$ .

The spatial structure of the acousto-optic effect in the case of the pure shear elastic mode propagating along a direction corresponding to the angles  $\varphi_a = 30^0$  and  $\vartheta_a = 63.5^0$  is shown in Fig. 15. It is seen in the picture that the spatial structure of this effect dramatically differs from the acousto-optic effect in Fig. 10. The explanation of the found trend is quite evident. The tensor of the photoelastic coefficients of tellurium  $\hat{\mathbf{p}}$  is characterized by a lower spatial symmetry compared to the tensor of the elastic constants [8,9,24,25]. That is why, the planes  $YZ$  and  $X+30^0$  that are identical from the point of view of the elastic properties, nevertheless, possess different magnitudes of the acousto-optic effect.

In the examined plane of the interaction, the maximal value of the acousto-optic figure of merit is obtained if the extraordinary polarized radiation is propagating along the direction with the angles  $\varphi_o = 18^0$  and  $\vartheta_o = 86^0$ . In particular, the maximal figure of merit in the plane  $X+30^0$  is equal to  $M_2 = 141\,900 \cdot 10^{-18} \text{ s}^3 / g$ , which is 4.3 times higher than in the plane  $YZ$  of the material. The matching condition is provided by the acoustic waves with the frequency  $f = 164$  MHz while the Bragg angle in the examined geometry is equal to  $\vartheta_B = 64.7^0$ . However, a cut of the crystal corresponding to the latter case is rather complicated because the interaction plane forms a different form zero angle relatively to the optical axis  $Z$ . The picture in Fig. 15, a proves this statement. In the picture, the points A and O show the directions of the acoustic and optic propagation in the coordinate plane including the angles  $\varphi$  and  $\vartheta$  while the line connecting these points belongs to the plane of the acousto-optic interaction. The frequency dependence of the Bragg angle is presented in Fig. 16, where the bold dot demonstrates the optical interaction geometry, at which the maximal figure of merit value  $M_2 = 141\,900 \cdot 10^{-18} \text{ s}^3 / g$  is observed.

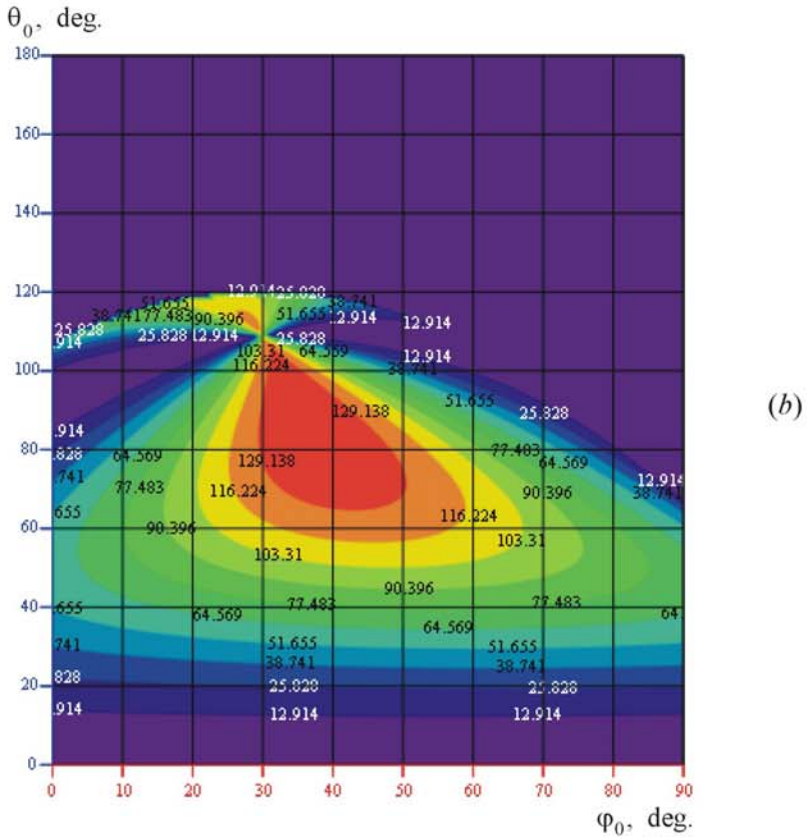
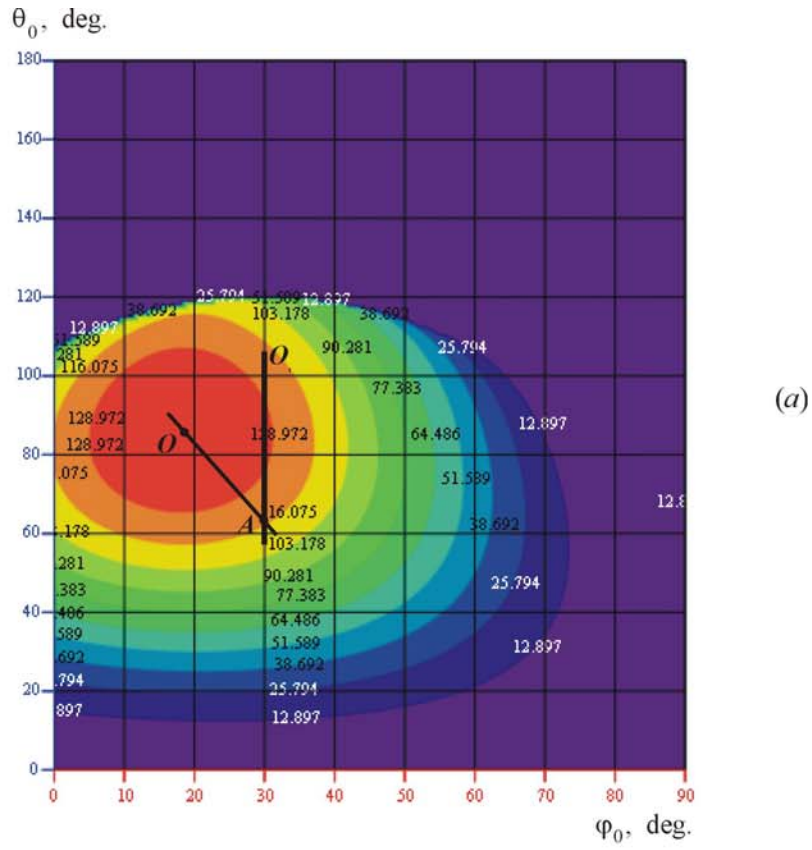


Figure 15. Spatial structure of AO effect for shear acoustic wave at  $\phi = 30^\circ$  and  $\theta = 63.5^\circ$

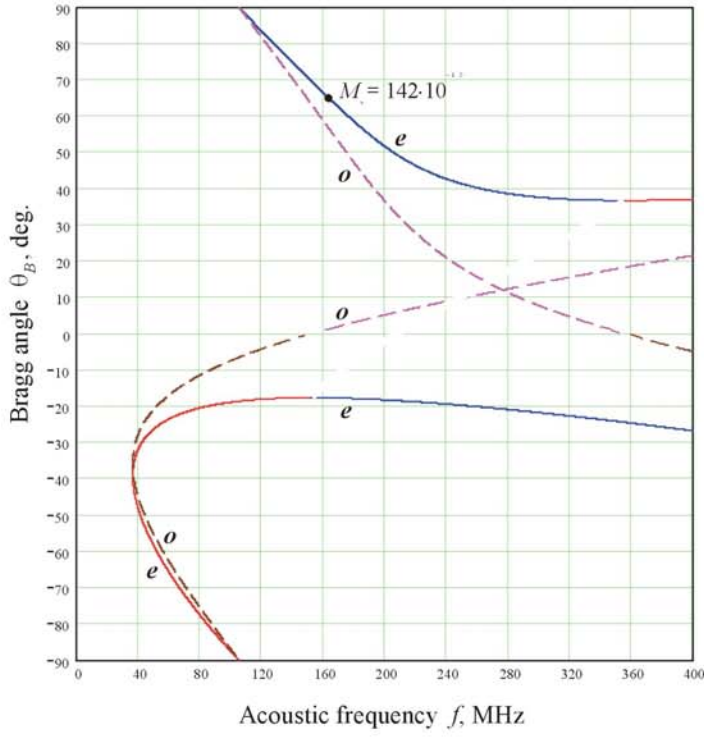


Figure 16. Frequency dependence of Bragg angle at propagation of sound at  $\varphi = 18^\circ$  and  $\theta = 16^\circ$

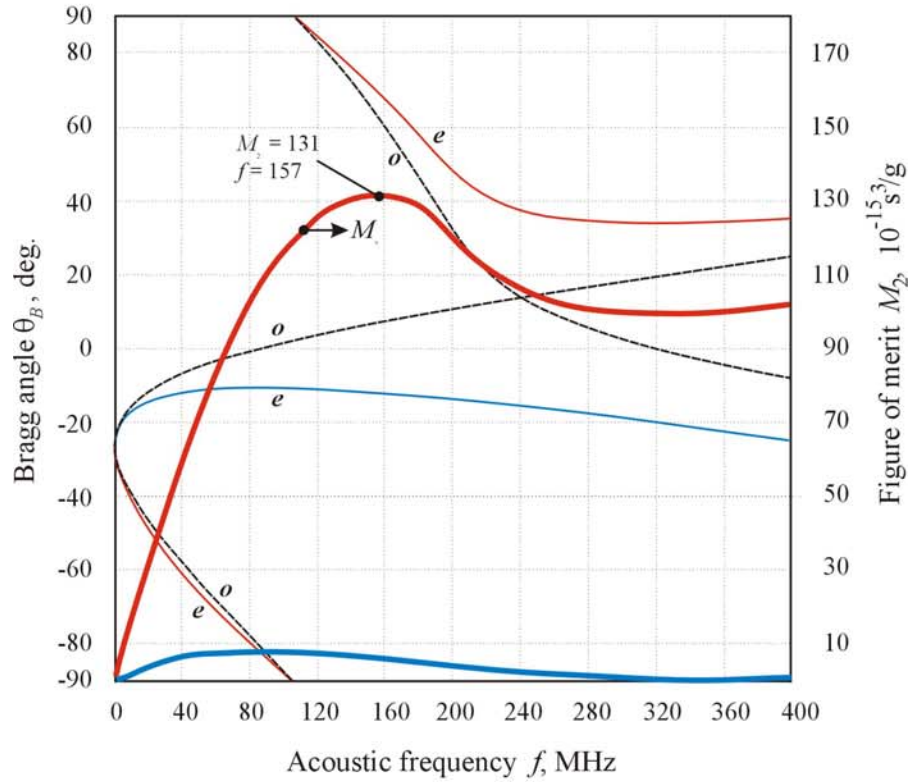


Figure 17. Frequency dependence of Bragg angle and figure of merit in case of acoustic propagation in  $X+30^\circ$  plane

A more convenient geometry of the diffraction is characteristic of the case when the plane of the interaction coincides with the plane  $X+30^0$ . In Fig. 15, the plane  $X+30^0$  is shown by the vertical line OA. It is evident that the acousto-optic figure of merit in this case is lower, however, a decrease in the diffraction efficiency is not so noticeable, e.g. of the order of 7.5%. The frequency dependence of the Bragg angle is similar to the dependence of the Bragg angle in the plane YZ (Fig. 13, a). The general view of the frequency dependence  $M_2(f)$  in Fig. 17 demonstrates no differences compared to the dependence in Fig. 13. However, the absolute magnitudes of the figure of merit plotted in Fig. 17 are much higher than the magnitudes in Fig. 13. As found, by the calculations, the maximum value of the acousto-optic figure of merit in the plane  $X+30^0$   $M_2 = 131\,200 \cdot 10^{-18} \text{ s}^3 / g$  is observed at the acoustic frequency  $f = 160 \text{ MHz}$ . The Bragg angle of light incidence and the diffraction angle are correspondingly equal to  $\vartheta_B = 68.5^0$  and  $\vartheta_d = 61.6^0$ . The corresponding vector diagram describing the optimal acousto-optic interaction is presented in Fig. 18. It is worth pointing out that this interaction geometry is very close to the collinear geometry of light diffraction. Unfortunately, it was found that this diffraction regime is not suitable for the application in the wide angle tunable filters intended for processing of images.

## 7. Trade-off between figure of merit and optical propagation direction

Based on the consideration presented above, the following directions of analysis were chosen in the present research program. According to the goals of the research program, it was necessary to find an acousto-optic interaction geometry in tellurium possessing slightly lower magnitudes of the figure of merit but, nevertheless providing the wide angle diffraction regime in the crystal. Similar to the tellurium dioxide single crystal [1,3,4,27], this geometry of interaction may be found at the angles of acoustic propagation  $\vartheta_a$  close to  $90^0$ . However, data in Fig. 14 prove that the far-off-axis cases of the interaction correspond to the large acoustic walkoff angles  $\alpha$ . Fortunately, the acoustic walkoff angles belong only in the plane  $X+30^0$ . This feature of the crystal is of importance since it indicates that the plane of the acousto-optic interaction should coincide with the plane  $X+30^0$  of the material.

In Fig. 19, the curve of the walkoff angle dependence  $\alpha(\vartheta_a)$ , similar to that shown in Fig. 14, is plotted together with the dependence of the maximal value of the figure of merit  $M_2$ . It is seen in the picture that the maximum value of the coefficient  $M_2 = 142\,900 \cdot 10^{-18} \text{ s}^3 / g$  may

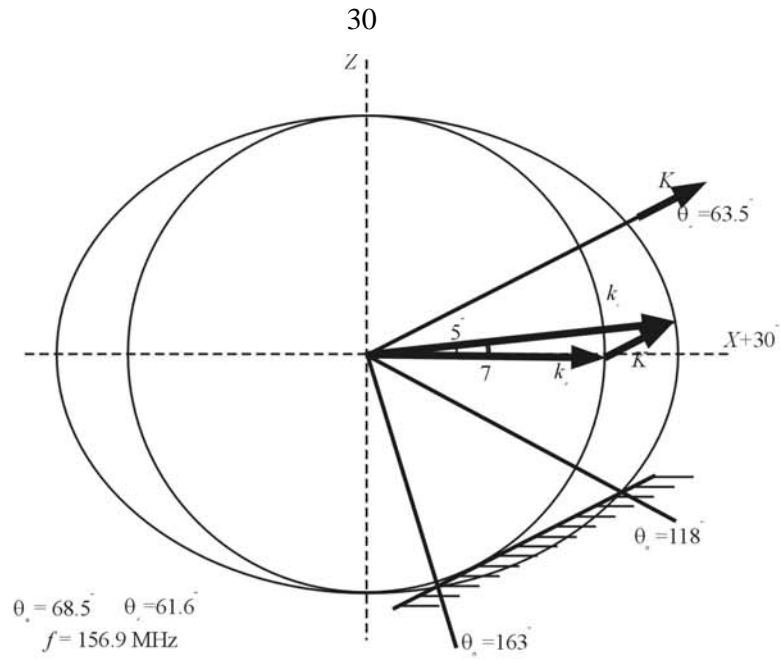


Figure 18. Wave vector diagram in  $X+30^\circ$  plane of tellurium

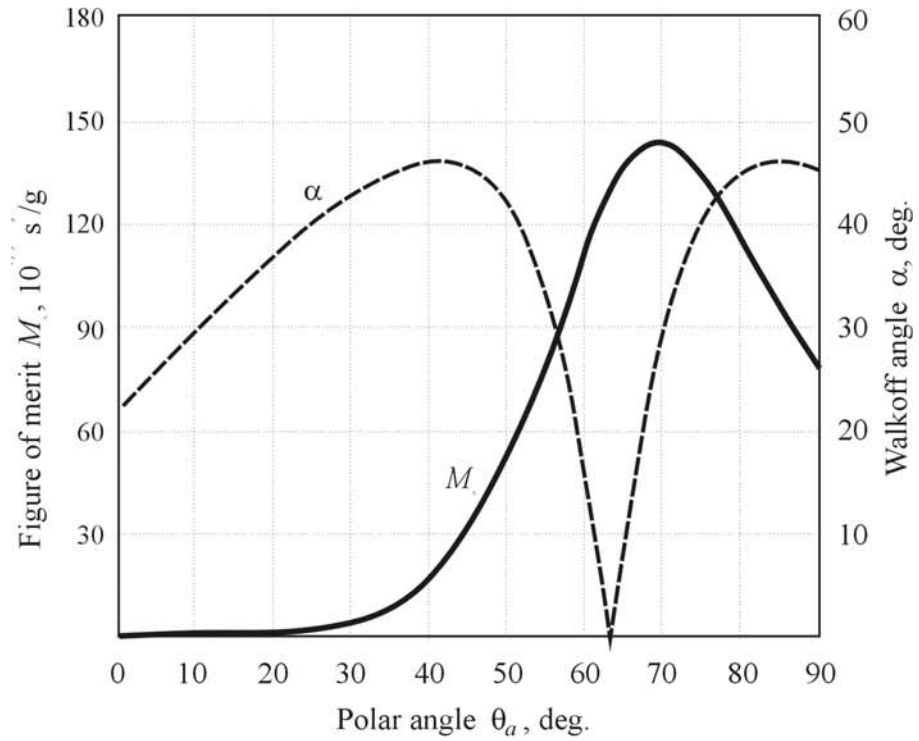


Figure 19. Acoustic walkoff angle and figure of merit versus acoustic propagation angle in  $X+30^\circ$  plane in tellurium

Table 1

$\theta_a$	$\alpha$	$M_2, 10^{-18}$ $s^3/g$	$V, 10^5$ $cm/s$	$\theta_0$	$\theta_B$	$\theta_d$	$f, MHz$
$0^0$	$23.7^0$	0	2.38				
$20^0$	$37^0$	330	1.95	$47^0$	$63^0$	$59^0$	678
$30^0$	$43^0$	3 700	1.69	$72^0$	$48^0$	$32.5^0$	305
$40^0$	$46^0$	16 740	1.42	$79^0$	$51^0$	$36^0$	264
$50^0$	$42^0$	52 740	1.19	$83^0$	$57^0$	$45^0$	204
$60^0$	$17^0$	113 560	1.06	$85^0$	$65^0$	$57^0$	164
$63.5^0$	0	131 240	1.054	$85^0$	$68.5^0$	$61.6^0$	156.9
$67^0$	$18^0$	141 330	1.06	$85^0$	$72^0$	$66^0$	154
$70^0$	$29^0$	142 900	1.09	$86^0$	$74^0$	$69^0$	156
$72^0$	$34^0$	140 590	1.11	$86^0$	$76^0$	$72^0$	157
$75^0$	$40^0$	133 190	1.16	$86^0$	$79^0$	$76^0$	161
$80^0$	$45^0$	114 790	1.26	$86^0$	$84^0$	$82^0$	172
$85^0$	$46^0$	94 700	1.37	$87^0$	$88^0$	$87^0$	187
$90^0$	$45^0$	76 610	1.50	$88^0$	$88^0$	$87^0$	205

Parameters of acousto-optic interaction in  $X+30^0$  plane of tellurium

be obtained if the shear acoustic wave is launched in the crystal along the direction at the angle  $\vartheta_a = 70^\circ$ . The acoustic walkoff angle of this wave is equal to  $\alpha = 29^\circ$ . As for detailed information about other regimes of the acousto-optic interaction typical of the plane  $X+30^\circ$ , they are summarized in the Table 1. In the Table 1, each direction of the acoustic propagation, i.e. each value of the angle  $\vartheta_a$  is described by the acoustic walkoff angle  $\alpha$  and the acoustic velocity  $V$ , as well as by the figure of merit  $M_2$ . Moreover, data in the Table 1 helps to find directions of the optimal polar incidence angle  $\vartheta_o$  so as the Bragg  $\vartheta_B$  and the diffraction  $\vartheta_d$  angles in the crystal. Finally, the corresponding acoustic frequency values  $f$  are also included in the Table 1.

Data in Fig. 20 show a family of frequency dependences of the Bragg angle in the case of the extraordinary polarized radiation and high values of AO efficiency in the crystal. Different curves in the figure correspond to the different values of the acoustic propagation angle  $\vartheta_a$  in the plane  $X+30^\circ$  of the crystal. The bold dots in the picture indicate the region of the incidence angles, at which the maximum values of the figure of merit may be observed. It is seen in the figure that the most promising, for the imaging application, geometry of wide angle interaction exists at the acoustic propagation angle  $\vartheta_a = 75^\circ$  because  $d^2 f / d\vartheta^2 = 0$  [1-4,27]. The case with the equal to zero second derivative of the frequency is observed at the frequency of ultrasound  $f = 175$  MHz, The extremely wide range of the incidence angles, i.e. from  $\vartheta_B = 25^\circ$  to  $\vartheta_B = 90^\circ$ , satisfy the phase matching condition at this frequency of ultrasound. Consequently, exactly this regime of the acousto-optic interaction requires a thorough examination.

Spatial structure of the acousto-optic effect, observed during the diffraction of the optical beams by the slow shear acoustic wave propagating in the direction corresponding to the angles  $\varphi_a = 30^\circ$  and  $\vartheta_a = 75^\circ$ , is presented in the Fig. 21. The maximal value of the acousto-optic figure of merit equal to  $M_2 = 142\,600 \cdot 10^{-18} \text{ s}^3 / g$  is obtained if the extraordinary polarized radiation is propagating at the angles  $\varphi_o = 19^\circ$  and  $\vartheta_o = 87^\circ$ . However, this interaction geometry is not convenient for the design of the acousto-optic devices because the acoustic wave possesses, in the plane  $X+30^\circ$ , the strong walkoff characterized by the angle  $\alpha = 40^\circ$ . However, it was found that the plane of the interaction could be slightly changed without losses in the figure of merit. For example, if the plane coincides with the plane  $X+30^\circ$  then the maximum

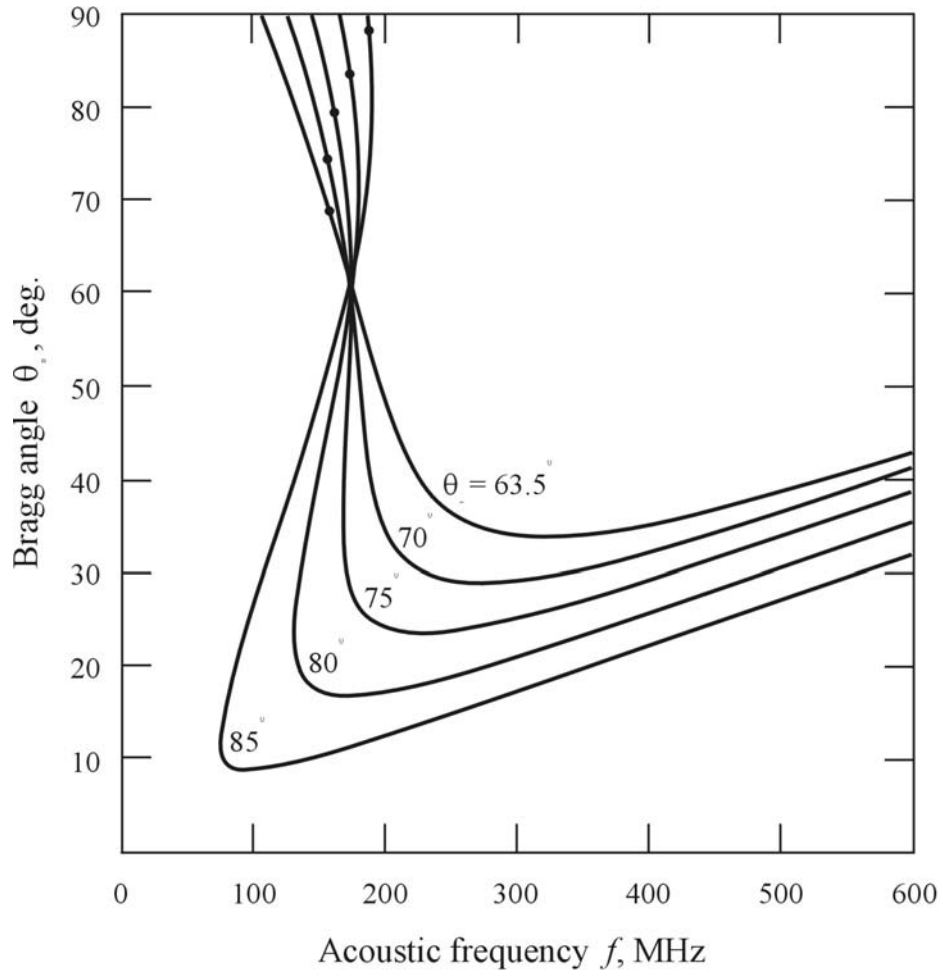


Figure 20. Family of frequency dependences of Bragg angle in  $X+30^\circ$  plane

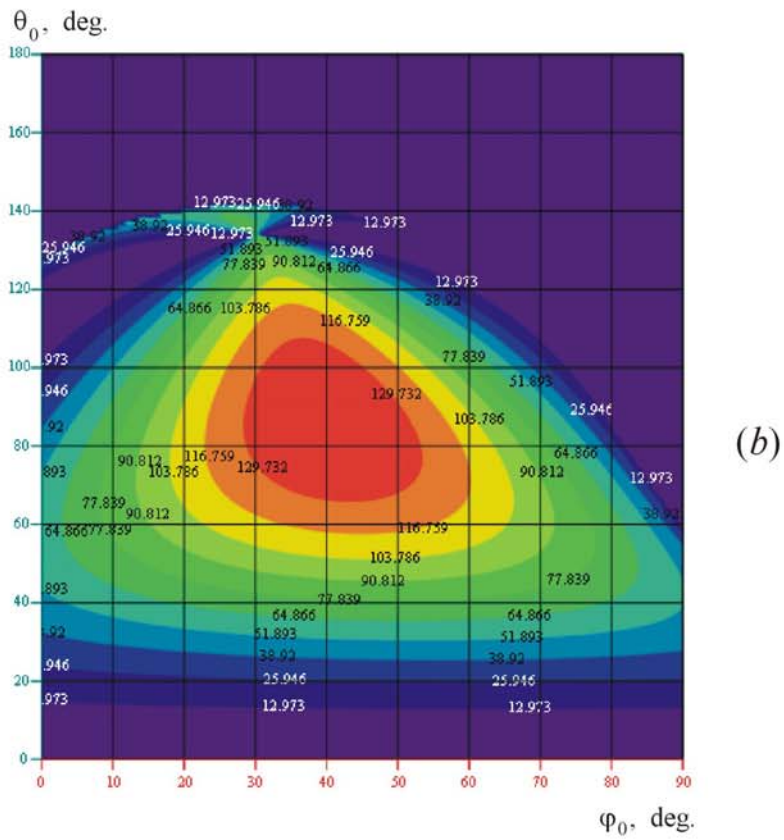
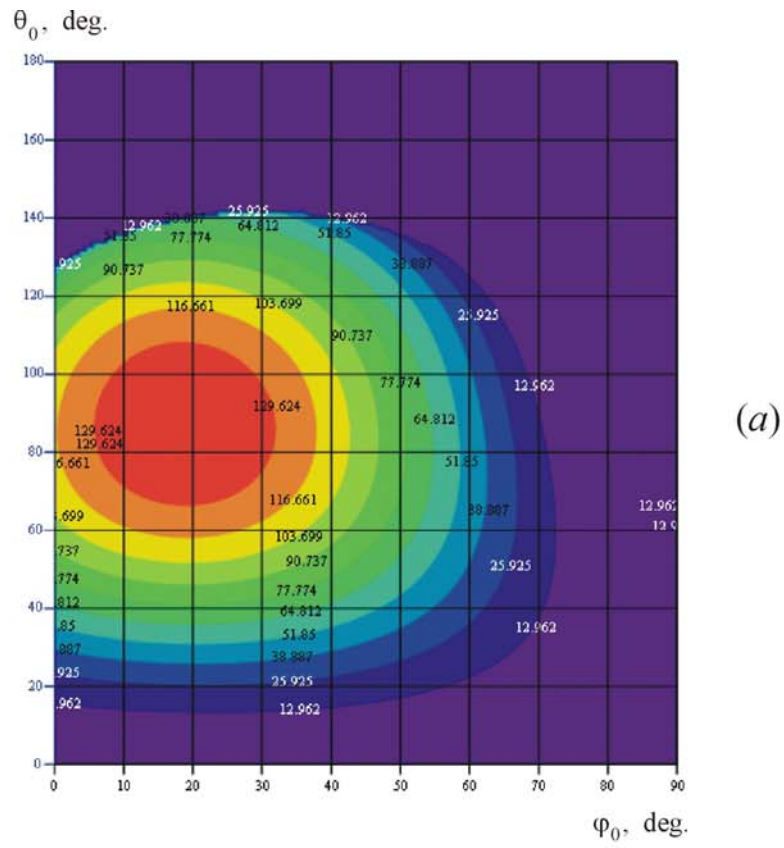


Figure 21. Spatial structure of AO effect in  $X+30$  plane at  $\varphi = 30^\circ$  and  $\theta = 75^\circ$

magnitude of the acousto-optic figure of merit, as follows from the Table 1, becomes equal to  $M_2 = 133\,200 \cdot 10^{-18} \text{ s}^3 / \text{g}$  that is only 7% lower than in the optimal case.

The dependence of the Bragg angle on the acoustic frequency all over the examined range of the acousto-optic interaction in tellurium is presented in Fig. 22. As for the data in Fig. 23, they correspond to the most interesting low-frequency branch of the frequency characteristics. The dependence of the coefficient  $M_2(f)$  on the acoustic frequency is also plotted in the picture. The picture in Fig. 23 includes the colours of the curves that are similar to those in the Fig. 17 and Fig. 13. It was noticed that, in the range of the acoustic frequencies  $f > 165$  MHz, the dependence  $M_2(f)$  was by chance characterized by a similar shape compared to the frequency curve  $\mathcal{G}_B(f)$ . It means that the second power of the photoelastic coefficient  $p_{eff}$  determining the figure of merit is changing in the crystal proportionally to the Bragg angle  $\mathcal{G}_B$ . In other words, the analysis revealed the regular trend that, in the region of the wide angle diffraction, there exists a strong dependence of the figure of merit on choice of an operating point on the angular characteristics. Consequently, the diffraction depends on the particular value of the Bragg incidence angle  $\mathcal{G}_B$ . For example, at the incidence angle  $\mathcal{G}_B = 70^\circ$ , the acousto-optic figure of merit in tellurium is equal to  $M_2 = 131\,100 \cdot 10^{-18} \text{ s}^3 / \text{g}$ . However, if the incidence angle is adjusted to  $\mathcal{G}_B = 30^\circ$  then the acousto-optic efficiency decreases to  $M_2 = 71\,700 \cdot 10^{-18} \text{ s}^3 / \text{g}$ . It is really amazing that the acoustic frequency corresponding to the condition of Bragg phase matching remains practically unchanged and equal to  $f = 170$  MHz in the wide variety of the incidence angles.

Examining a particular design of the acousto-optic cell operating on base of the chosen acoustic mode, it is also necessary to consider the walkoff of the elastic energy. As found, the acoustic walkoff angle  $\alpha$  has a positive sign in the case of the examined crystal cut. It means that the acoustic column is tilted towards the plane XZ. Moreover, this walkoff angle appears at  $\mathcal{G}_a = 75^\circ$  as large as  $\alpha = 40^\circ$ . For better understanding of the obtained results of the research, the drawing in Fig. 24 presents various configurations of the acousto-optic cells that may be developed on base of the chosen cut of the material. The cells correspond to different operating points at the frequency characteristics of the incidence angle  $\mathcal{G}_B(f)$ . These operating points may be easily seen in Fig. 23.

The regime of the acousto-optic interaction shown in Fig. 24 (a) corresponds to the collinear diffraction when all the three wave vectors  $\mathbf{k}_i$ ,  $\mathbf{k}_d$  and  $\mathbf{K}$  possess one and the same

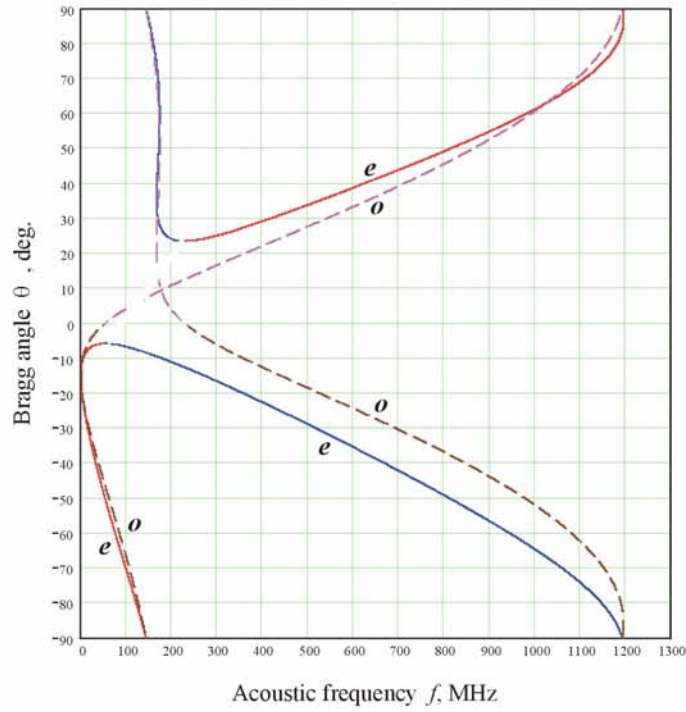


Figure 22. General view of Bragg angles frequency dependence at acoustic propagation  $\varphi = 30^\circ$  and  $\theta = 75^\circ$

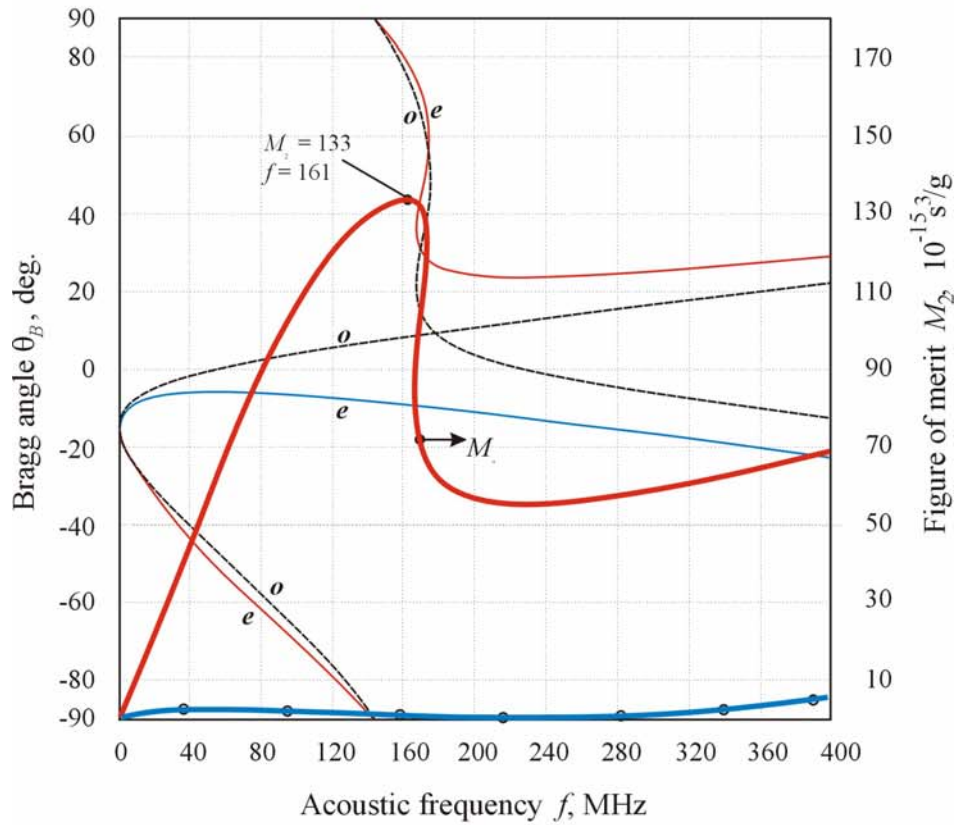


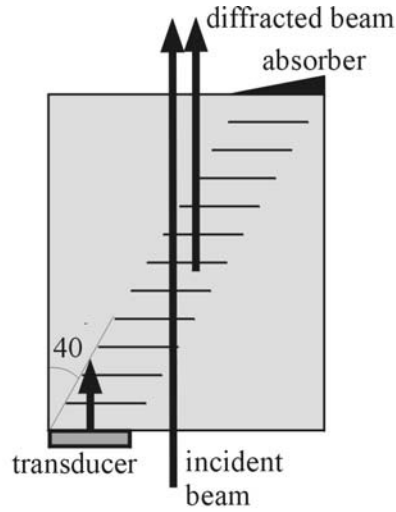
Figure 23. Frequency dependences of Bragg angles and figure of merit at acoustic propagation  $\varphi = 30^\circ$  and  $\theta = 75^\circ$

direction of propagation [1-4]. Due to the elastic energy walkoff, propagation of light through the acoustic column may be provided without difficulties. In the collinear configuration, the acoustic frequency and the acousto-optic figure of merit are correspondingly equal to  $f = 144$  MHz and  $M_2 = 130100 \cdot 10^{-18} \text{ s}^3 / \text{g}$ . However, it is also necessary to take into account the fortunate increase in the real interaction length to a factor of  $1/\text{tg}\alpha$ . As a result, the effective figure of merit value of the crystal cut appears equal to  $M_2^* = 184700 \cdot 10^{-18} \text{ s}^3 / \text{g}$ .

The configuration of the cell presented in Fig. 24 (b) corresponds to the Bragg incidence angle  $\vartheta_B = 70^\circ$ . The acoustic frequency and the acousto-optic figure of merit characteristic of this design of the cell are equal to  $f = 170$  MHz and  $M_2^* = 131100 \cdot 10^{-18} \text{ s}^3 / \text{g}$ . This diffraction geometry is just the required wide angle anisotropic interaction. However, the configuration in Fig. 24 (b) is not convenient for the application because both the incident and the diffracted optical beams propagate through the crystal very close to the acoustic energy flow. Therefore, there exists a problem how to direct the incident optical beam into the acoustic column [26-28]. On the other hand, mirror geometry of interaction shown in Fig. 24 (c) may also be observed in the crystal. In the latter case, the acoustic frequency is equal to  $f = 99$  MHz while the figure of merit is decreased to  $M_2^* = 104900 \cdot 10^{-18} \text{ s}^3 / \text{g}$ . Unfortunately, the mirror geometry in tellurium may not be defined as the wide angle diffraction so that the diffraction is not suitable for the application.

Finally, the acousto-optic cell in Fig. 24 (d) utilizes the diffraction taking place at the incidence angle  $\vartheta_B = 30^\circ$ , for which the acoustic frequency is equal to  $f = 170$  MHz and the figure of merit approaches the value  $M_2 = 70500 \cdot 10^{-18} \text{ s}^3 / \text{g}$ . Due to the inclined propagation of the optic wave through the acoustic column, the effective figure of merit in the cell is improved by the acoustic walkoff to a factor of 1.5, i.e.  $M_2^* = 109500 \cdot 10^{-18} \text{ s}^3 / \text{g}$ . This value of the figure of merit in tellurium may be considered as quite tolerable for the imaging applications. Consequently, this cut of the crystal may be recommended for further examination and usage.

The performed investigation demonstrated that some kind of trade-off should be taken into consideration between the diffraction efficiency and the figure of merit, on the one hand, and the direction of light propagation relatively the axis Z and the absorption of light, on the other hand. As mentioned, propagation of the infrared radiation close to the optical axis in the

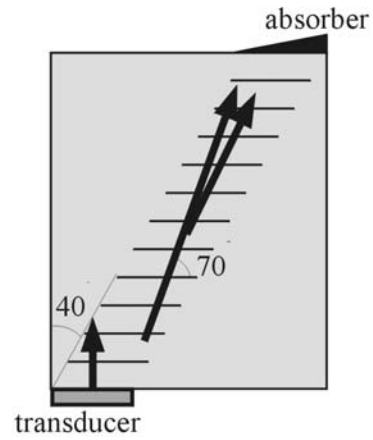


(a) Collinear geometry

$$f = 144 \text{ MHz}$$

$$M_v = 130 \cdot 10^{-3} \text{ s/g}$$

$$M_v^* = 185 \cdot 10^{-3} \text{ s/g}$$

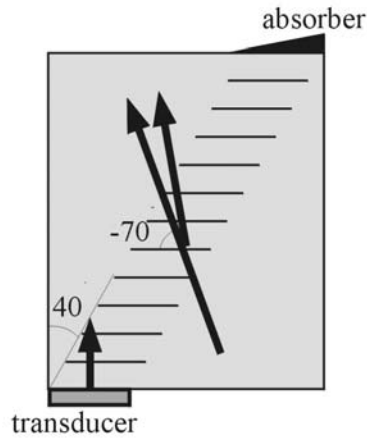


(b) Wide angle geometry

$$f = 170 \text{ MHz}$$

$$M_v = 131 \cdot 10^{-3} \text{ s/g}$$

$$\theta_v = 70 \quad \theta_j = 64$$

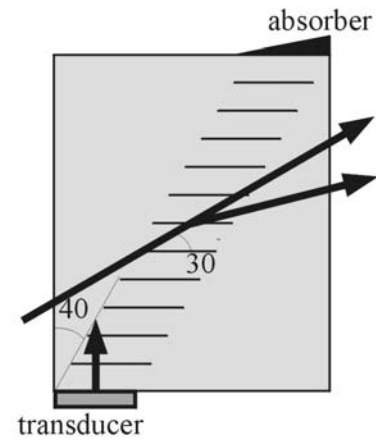


(c) Narrow angle geometry

$$f = 144 \text{ MHz}$$

$$M_v = 105 \cdot 10^{-3} \text{ s/g}$$

$$\theta_v = -70 \quad \theta_j = -64$$



(d) Wide angle geometry

$$f = 170 \text{ MHz}$$

$$M_v = 71 \cdot 10^{-3} \text{ s/g}$$

$$M_v^* = 110 \cdot 10^{-3} \text{ s/g}$$

$$\theta_v = 30 \quad \theta_j = 14$$

Figure 24. Configurations of acousto-optic cells

crystal of tellurium is accompanied by better transparency of the material, especially for the extraordinary polarized light. However this propagation corresponds to poor magnitudes of the figure of merit of the material. On the contrary, the far-off axis geometry possesses better diffraction efficiency but worse transparency. Fortunately, data in Fig. 23 prove that the wide angle interaction geometry exists in a wide variety of the incidence angles, where the second derivative of the dependence  $\mathcal{G}(f)$  is equal to zero. During a design of a cell, it gives flexibility in the selection of the cut of the crystal.

## 8. Summary of results of calculations

Operation points belonging to all the examined, in this report, regimes of the acousto-optic interaction are shown in Fig. 25. For simplicity, only the low-frequency branches of the Bragg angle characteristics are plotted in the figure. It is evident that the frequency curves in Fig. 25 correspond to the extraordinary polarized incident optical light. As mentioned, the most important result of the calculation consists in the statement that the high magnitudes of the figure of merit are observed in the single crystal of tellurium only if the optical waves propagate far away from the optical axis. The reason for this characteristic feature of the crystal lies in the feature that the magnitude of the photoelastic coefficient  $p_{41} = 0.28$  is superior to all other photoelastic coefficients providing the anisotropic diffraction [22]. In general, the carried out analysis proves that the anisotropic acousto-optic interaction is provided in tellurium by the photoelastic coefficients belonging to the fourth, fifth and sixth lines of the matrix of the constants  $p_{ij}$ . In particular, the absolute value of the coefficient  $p_{41}$  is 2 times higher than the magnitude of the coefficient  $p_{44}$  that may also be responsible for the anisotropic diffraction. It means that the figure of merit  $M_2$  of tellurium, in which the coefficient  $p_{41}$  is engaged, occurs about 4 times better than the corresponding  $M_2$  factor, in which the coefficient  $p_{44}$  is included.

There is one more aspect of the interaction that has to be taken into the consideration during a selection of the interaction geometry. It is necessary to satisfy the requirement that the acousto-optic interaction plane includes the optical axis of the birefringent crystal. This requirement is quite evident because the imaging filter must be capable of processing of two-dimensional images. That is why the wide angle geometry of interaction should be satisfied in the crystal in two orthogonal planes simultaneously, i.e. along two orthogonal directions in space. It is known that the condition of the two-dimensional interaction is most easily satisfied in a birefringent material if the interaction plane includes the optical axis  $Z$ . In this respect, the non-

symmetrical interaction geometry of the deflector proposed in the reference [30] may hardly be utilized in the instrument intended for the processing of images.

It is quite clear that the acousto-optic interaction geometry in the single crystal of tellurium with the far-off-axis propagation of light becomes reasonable only in specimens with good optical transparency. Consequently, the result of this investigation, to a great extent, depends on the possibility to grow the birefringent material with low absorption of the optical radiation in the long infrared region of spectrum.

## 9. Growth and characterization of tellurium specimens

According to the Program of the research, the scientific group from the A.F.Ioffe Institute in St. Petersburg performed a detailed literature survey on techniques to find out the optimal way to grow boules of the single crystals of tellurium. Later the boules of tellurium were grown in quartz ampoules by Bridgman method. The crystals were obtained in form of hexagonal cylinders about 1 cm in diameter and up to 2.5 cm long.

The material was examined by means of X-ray analysis in order to determine the directions of the crystalline axes. The analysis showed that the optical axis  $Z$  was directed orthogonal to the diameter of the boules. After the axes were identified, the boules were cut in form of rectangular prisms and in form of optical phase plates with orientation along the crystalline axes  $X$ ,  $Y$  and  $Z$ . The positive and the negative directions of the axes were also determined during the preliminary characterization of the samples. As found experimentally, the grown crystals belonged to the **left modification** of the material.

Optical absorption in the grown samples evaluated by means of a carbon dioxide laser at the wavelength of light  $\lambda = 10.6$  mkm. It was found that the Fresnel losses of the crystal were extremely high because of the large magnitudes of the refraction indexes ( $n_o = 4.8$  and  $n_e = 6.2$ ) for both the ordinary and the extraordinary polarized beams. It makes it possible to predict that transmission of a perfectly polished thin plate of tellurium at normal incidence of light is equal to about  $T = 40\%$  for the ordinary wave and to  $T = 30\%$  for the extraordinary polarized radiation. On the other hand, it is evident that the Fresnel losses may be sufficiently decreased if antireflection coatings are used in a cell.

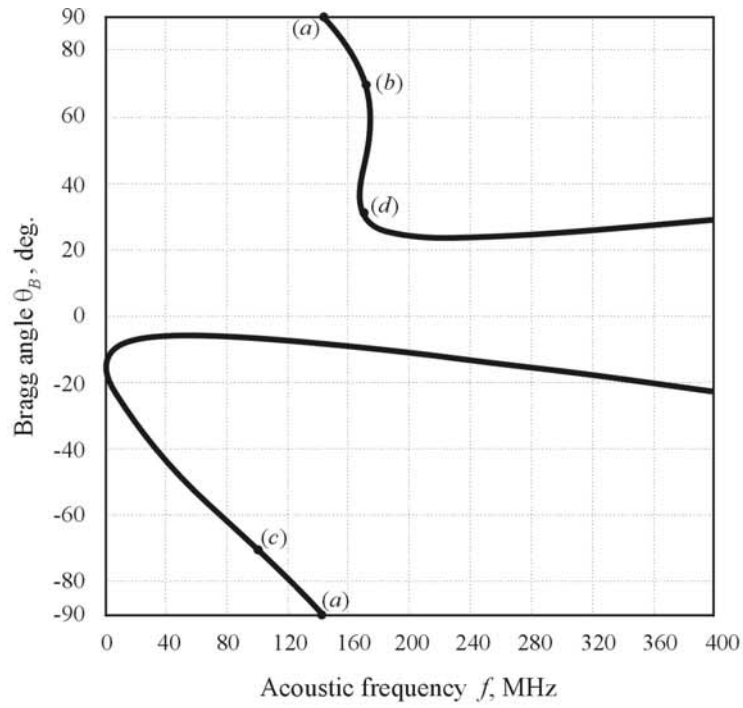


Figure 25. Operation points at frequency dependences in  $X+30^\circ$  plane of tellurium

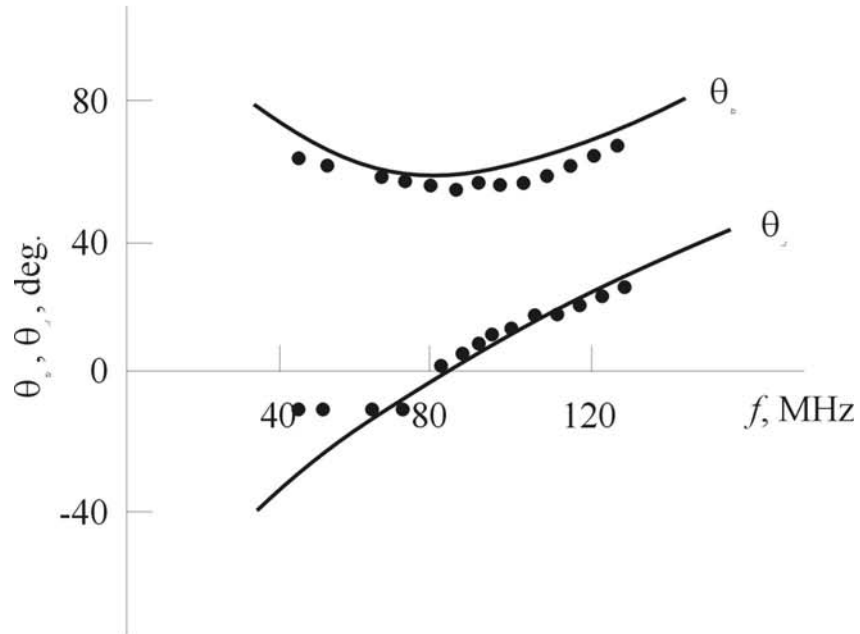


Figure 26. Measured frequency dependences of Bragg angle at 10.6 mkm

In order to evaluate quantitatively the attenuation coefficient in tellurium, the specimens were cut in form of thin plates with thickness about 0.4 cm. The plates were fabricated orthogonal to  $Z$  axis and to  $X$  or  $Y$  axes of the crystal. The measurement demonstrated that the optical radiation sent along the optical axis  $Z$  was transmitted with the relative intensity at the output of the crystal included in the limits from 20% to 30%. Consequently, the optical absorption coefficient in tellurium was equal to  $1.0 - 1.5 \text{ cm}^{-1}$ . The Fresnel reflection and the intrinsic attenuation in the material, which additionally decreased the optical intensity to a factor of 1.3 - 2.0, were taken into account during the measurement of the attenuation.

Absolutely opposite result was obtained in the case of the extraordinary polarized radiation sent along  $X$  and  $Y$  axis of the crystal. It was recorded that the total transparency of the crystal was as low as  $T = 0.5 - 1.0 \%$ . It means that the absorption coefficient of tellurium in this case occurs equal to  $8.5 - 10.0 \text{ cm}^{-1}$ . The Fresnel losses resulted in the decrease of the optical intensity to about 70% while, in the material itself, the radiation was additionally attenuated to a factor of 50. These losses were considered as not tolerable for the application. Therefore, the techniques of the crystal growth should somehow be improved. This improvement is planned for the next period of the research. Moreover, it may be expected that cooling of the crystal and application of the antireflection coatings will definitely decrease the attenuation of light.

In order to verify the conclusions of the theoretical analysis relayed to the characteristic features of the anisotropic diffraction, a prototype acousto-optic cell was fabricated in the A.F.Ioffe Institute. Operation of the cell was based on the diffraction of light by the slow shear acoustic wave propagating in the  $YZ$  plane of the crystal at the angle  $\vartheta = -26^\circ$  with respect to the axis  $Y$ . Polarization of the acoustic wave was directed along  $X$  axis, therefore, this acoustic mode could be defined as a pure acoustic mode [8,17].

It should be noted that the geometry of the acousto-optic interaction corresponded to the deflector configuration of the cell and not the imaging filter configuration. This interaction is represented in Fig. 13 by the point A. The special choice of the deflector configuration instead of the filter configuration was explained by the following reasons. It was decided to characterize the crystal as a birefringent material, to verify its particular modification (left) and to determine directions (positive or negative) of the axes in the crystals. It was also necessary to check the material in the relatively simple geometry of light and sound interaction characterized by

propagation of the optic waves close to the axis  $Z$ , where the optical losses of tellurium for both optical modes are low.

Data in Fig. 25 demonstrate the measured dependence of the Bragg angle of light incidence on the frequency of the acoustic wave in the crystal. The measurement was performed at the wavelength of light  $\lambda = 10.6$  mkm by means of a carbon dioxide laser. Comparison of data in Fig. 13 and Fig. 25 shows that the general view of the frequency curves illustrating the angles of optical incidence and diffraction is in good agreement with the predictions of the theory. The measured acoustic frequency  $f = 83$  MHz, at which the extreme value of the Bragg angle for the extraordinary polarized light was registered, only slightly differed from the theoretical value  $f = 86$  MHz. It means that the acousto-optic interaction in tellurium took place in accordance with the expectations. The positive direction of the crystalline axes and the left modification of the crystal were in this way confirmed in the experiment. As for the efficiency of diffraction, measurement of the diffracted light intensity demonstrated that the figure of merit of tellurium was low. However, it was absolutely not surprising because the figure of merit of the crystal in the applied cut of tellurium is really poor because the radiation was sent in the crystal close to the optical axis.

## 10. CONCLUSIONS

The performed investigation proves that the single crystal of tellurium is one of the best materials for application in the imaging acousto-optic filters operating in the long infrared region of spectrum at the optical wavelengths  $\lambda = 8 - 12$  mkm. The material is superior to all other known infrared materials if the acousto-optic figure of merit is taken into consideration. The carried out theoretical investigation demonstrated that the crystal is optically and elastically anisotropic. It is characterized by a complicated character of propagation of the acoustic waves, especially along far-off-axis directions belonging to the planes that do not coincide with the basic planes of the material. As a result of the investigation, detailed information was obtained about the longitudinal and shear waves propagation in the crystal. The investigation was also concentrated on a thorough study of the photoelastic and acousto-optic properties of the material. As a result of the analysis, geometry of light and sound interaction optimal for the application in the imaging filter was found.

First specimens of the single crystal of tellurium have been grown according to the program of the research. The single crystals were obtained in quartz ampoules by Bridgman

method. The crystals belonged to the so-called left modification of the material. Optical transparency of the specimens was measured in a laser experiment. As found, the absorption of the first samples was poor indicating that it was necessary to improve the techniques of the growth of the crystal. Acousto-optic cell applying the anisotropic diffraction of light by ultrasound was fabricated on base of the grown crystal. Measurement of parameters of the anisotropic diffraction in the cells demonstrated that the registered data were in good agreement with the predictions of the theory.

### LITERATURE CITED

1. V.I.Balakshy, V.N.Parygin and L.E.Chirkov, *Physical Principles of Acousto-Optics*, Moscow: "Radio I sviaz", 1985 (in Russian).
2. A.Korpel, *Acousto-Optics*, 2nd ed. N.Y.: Artech House, 1997.
3. J.P.Xu and R.Stroud, *Acousto-optic Devices: Principles, Design and Applications*, N.Y.: Wiley & Sons Inc., 1992.
4. A.Goutzoulis and D.Pape, *Design and Fabrication of Acousto-Optic Devices*, N.Y.: Marcel Dekker Inc., 1994.
5. N.Uchida and N.Niizeki, Acoustooptic deflection materials and techniques, *Proc. IEEE*, 1973, v. 61, #8, p. 1073-1092.
6. R.W.Dixon and A.N.Chester, An acoustic light modulator for  $10,6\mu$ , *Appl. Phys. Letts.*, 1966, v. 9, #5, p. 190-192.
7. J.D.Feichtner, M.Gottlieb and J.J.Conroy,  $Tl_3AsSe_3$  noncollinear acousto-optic filter operation at  $10\mu m$ , *Appl.Phys. Letts.*, 1979, v. 34, # 1, Oxford: Clarendon Press, 1964.
8. B.A.Auld. *Acoustic Fields and Waves in Solids*, N.Y.: R.Krieger Publ. Company, 1990.
9. E.Dieulesaint et D.Royer, *Ondes elastiques dans les solides*, Paris: Mason, 1974.
10. I.C.Chang and P.Katzka, Acousto-optic properties of halcogenide compounds, *IEEE Ultrasonics Symposium*, 1987, p. 511-514.
11. D.Suhre and E.Villa, Imaging spectroradiometer for the 8–12mkm region with  $3\text{ cm}^{-1}$  passband acousto-optic tunable filter, *Appl. Opt.*, 1998, v. 37, # 12, p. 2340-2345.
12. M.Gottlieb, A.Goutzoulis and N.Singh, Mercury chloride ( $Hg_2Cl_2$ ) acousto-optic devices, *Proc. IEEE Ultrasonics Symposium*, 1986, p. 423-427.
13. M.Gottlieb, A.Goutzoulis and N.Singh, High-performance acousto-optic materials:  $Hg_2Cl_2$  and  $PbBr_2$ , *Opt. Eng.*, 1992, v. 31, p. 2110-2117.
14. I.M.Silvestrova, C.Barta, G.Dobrschansky, L.Belyaev and Yu.Pisarevsky, Acousto-optic properties of calomel crystal  $Hg_2Cl_2$ , *Sov. Phys. Crystallography*, 1975, v. 20, p. 1062-1069.
15. R.W.Dixon, Photoelastic properties of selected materials and their relevance for applications to acoustic light modulators and scanners, *J. Appl. Phys.*, 1967, v. 38, # 13, p. 5149-5153.
16. M.I.Zussman, N.K.Maneshin, E.R.Moustel and V.N.Parygin, Acousto-optic modulator of light, *Sov.Radiotechnics and Electronics*, 1973, v. 18, # 6, p. 1203-1207.
17. A.M.Diakonov, Y.V.Ilisavsky, I.I.Farbstein et al., Efficient acousto-optic modulator on base of tellurium, *Sov. Tech. Phys. Letts.*, 1977, v .3, # 12, p. 564-567.
18. S.Fukuda, T.Shiosaki and A.Kawabata, Acousto-optic properties of tellurium at  $10.6\mu m$ , *J. Appl. Phys.*, 1979, v. 50, # 6, p. 3899-3995.
19. A.M.Diakonov, Y.V.Ilisavsky and E.Z.Yahkind, Investigation of acousto-optic interaction of IR radiation with sound in tellurium, *Sov. Tech. Phys. J.*, 1981, v. 51, # 7,

- p. 1494-1502.
20. J.Oliveira and E.Adler, Analysis of off-axis anisotropic diffraction in tellurium at  $10.6\ \mu\text{m}$ , *IEEE Trans.Ultrasonics, Ferroelectrics and Frequency Control*, 1987, v. UFFC-34, # 1, p. 86-94.
  21. P.Gorley, I.Kushnir and V.Shenderovsky, Acoustic and piezoelectric properties of tellurium single crystals, *Ukrainian J. Phys.*, 1989, v. 34, # 1, p. 102-109.
  22. D.Souilhac, D.Billeret and A.Gundjian, Photoelastic tensor of tellurium, *Appl. Opt.*, 1989, v. 28, # 18, p. 3993-3996.
  23. D.Suhre, L.Taylor and N.Melamed, Spatial resolution of imaging noncollinear acousto-optic tunable filters, *Opt. Eng.*, 1992, v. 31, # 10, p. 2118-2123.
  24. J.F.Nye. *Physical Properties of Crystals* Masson et C<sup>ie</sup>, 1974.
  25. Acoustic crystals. / Ed. by M.P.Shaskolskaya, Moscow: Nauka, 1982.
  26. V.B.Voloshinov, Close to collinear acousto-optical interaction in paratellurite, *Opt.Eng.*, 1992, v. 31, # 10, p. 2089-2094.
  27. V.B.Voloshinov, Anisotropic light diffraction on ultrasound in a tellurium dioxide single crystal, *Ultrasonics*, 1993, v. 31, # 5, p. 333-338.
  28. V.B.Voloshinov and D.D.Mishin, Quasicollinear diffraction of light by sound in a paratellurite crystal, *J. Commun. Techn. & Electronics*, 1993, v. 38, # 3, p. 42-48.
  29. D.Souilhac and D.Billerey, "Efficient acousto-optically tunable phase matched non collinear optical second harmonic generator on tellurium", *Proc. SPIE*, 1990, v. 1723, p. 162-173.
  30. D.Souilhac, D.Billerey and A.Gundjian, Infrared two-dimensional acousto-optic deflector using a tellurium crystal, *Appl. Optics*, 1990, v. 29, # 13, p. 1798-1804.
  31. D.Souilhac and D.Billerey, TeO<sub>2</sub> and Te spectrometer imaging system, *Proc SPIE*, 1993, v. 2312, p. 212-250.
  32. V.B.Voloshinov, Tunable acousto-optic imaging filter for 8-12 mkm region of spectrum, *Proposal on the Grant TRI-99-005* from the Technical Research Institute, 20484, Langley Drive, Sterling, Virginia 20165-3569, 2000.
  33. V.B.Voloshinov, Application of single crystals of  $Tl_3AsSe_3$  and  $Te$  in imaging filters operating at 8-12 microns, *Tech. Report #3 on the Grant TRI-01-N-002* from the Technical Research Institute, 20484 Langley Drive, Sterling, Virginia 20165-3569, 2002.
  34. V.B.Voloshinov, Acousto-optic effect in tellurium single crystal, *Technical Report #4* on the Grant TRI-02-N-003 from the Technical Research Institute, 20484, Langley Drive, Sterling, Virginia 20165-3569, 2004.
  35. V.B.Voloshinov, Acousto-optic interaction in single crystal of tellurium, *Proc. US-Russian Partnership Workshop CELO-2004* "Communication, Electronics, Laser and Optics", St. Petersburg, Russia, p. III-24, 2004.